energies

MDPI

Article

Modeling the Thermodynamics of Oxygen-Enriched Combustion in a GE LM6000 Gas Turbine Using CH_4/NH_3 and CH_4/H_2

Laith Mustafa [1], Rafał Ślefarski [2,*], Radosław Jankowski [2], Mohammad Alnajideen [3] and Sven Eckart [4]

[1] Department of Mechanical Engineering, University of Kansas, Lawrence, KS 66044, USA; laith.mustafa@ku.edu
[2] Institute of Thermal Engineering, Poznan University of Technology, 60-965 Poznan, Poland; radoslaw.jankowski@put.poznan.pl
[3] College of Physical Sciences and Engineering, Cardiff University, Cardiff CF24 3AA, UK; alnajideenmi@cardiff.ac.uk
[4] Institute of Thermal Engineering, TU Bergakademie Freiberg, 09599 Freiberg, Germany; sven.eckart@iwtt.tu-freiberg.de
* Correspondence: rafal.slefarski@put.poznan.pl; Tel.: +48-61-6652218

Abstract: Gas turbines are widely used in power generation due to their reliability, flexibility, and high efficiency. As the energy sector transitions towards low-carbon alternatives, hydrogen and ammonia are emerging as promising fuels. This study investigates the thermodynamic and combustion performance of a GE LM6000 gas turbine fueled by methane/hydrogen and methane/ammonia fuel blends under varying levels of oxygen enrichment (21%, 30%, and 40% O_2 by volume). Steady-state thermodynamic simulations were conducted using Aspen HYSYS, and combustion modeling was performed using ANSYS Chemkin-Pro, assuming a constant thermal input of 102 MW. Results show that increasing hydrogen content significantly raises flame temperature and burning velocity, whereas ammonia reduces both due to its lower reactivity. Net power output and thermal efficiency improved with higher fuel substitution, peaking at 43.46 MW and 42.7% for 100% NH_3. However, NO_x emissions increased with higher hydrogen content and oxygen enrichment, while NH_3 blends exhibit more complex emission trends. The findings highlight the trade-offs between efficiency and emissions in future low-carbon gas turbine systems.

Keywords: green hydrogen; ammonia; gas turbine cycle; alternative fuel; oxygen enriched combustion

Academic Editor: Albert Ratner

Received: 5 May 2025
Revised: 2 June 2025
Accepted: 12 June 2025
Published: 19 June 2025

Citation: Mustafa, L.; Ślefarski, R.; Jankowski, R.; Alnajideen, M.; Eckart, S. Modeling the Thermodynamics of Oxygen-Enriched Combustion in a GE LM6000 Gas Turbine Using CH_4/NH_3 and CH_4/H_2. *Energies* **2025**, *18*, 3221. https://doi.org/10.3390/en18123221

1. Introduction

The World Climate Action Summit (WCAS) aims to reduce CO_2 emissions by 22–25 gigatons of carbon dioxide equivalent $GtCO_2e$ by 2030 in order to keep warming below 1.5 °C [1]. The Paris Agreement aims to decarbonize the energy sector through lower consumption, lowering emissions from transportation, and improving energy security [2].

Switching from fossil fuels to renewables such as solar and wind presents issues, owing to their fluctuating nature. Because output is weather- and time-dependent, balancing supply and demand necessitates adequate energy storage. Intermittency can strain grid stability, threatening outages due to voltage and frequency changes [3].

Hydrocarbon-free fuels, such as ammonia and hydrogen, are becoming increasingly common. Hydrogen, at 121.1 MJ/kg, has a higher energy content than natural gas (48 MJ/kg), which improves efficiency in certain industries. Unlike fossil fuels, which release pollutants like CO_2, SO_x, NO_x, and particulate matter, hydrogen combustion produces solely water vapor, helping reduce greenhouse gas emissions and enhance air quality [4].

Hydrogen can be created through sustainable electrolysis powered by renewable energy sources such as hydroelectric, solar, or wind, resulting in "green hydrogen" with zero emissions. Hydrogen also improves energy security by lowering dependence on imported fossil fuels and diversifying energy sources, thereby increasing independence and resilience [5,6].

Hydrogen and renewable energy sources can be utilized to produce ammonia NH_3, mainly through the Haber–Bosch method [7]. Ammonia has a higher energy density per volume than hydrogen (12.69 MJ/L or 11.65 MJ/L, depending on storage conditions), and it can be kept as a liquid under manageable conditions, e.g., 1 bar at 240 K or 300 bar at 298 K [8]. These benefits make ammonia storage 26–30 times less expensive than hydrogen [7]. Table 1 shows that there are variations in energy content, flammability, and ignition properties between CH_4, H_2, and NH_3.

Table 1. Comparison of properties for CH_4, H_2, and NH_3 [9].

Property	CH_4	H_2	NH_3
Lower Heating Value—Mass (MJ/kg)	50.0	120.0	18.8
Lower Heating Value—Volume (MJ/m^3)	33.4	9.6	13.7
Adiabatic Flame Temperature (K)	2223	2483	1850
Lower Flammability Limit	0.5	0.1	0.63
Upper Flammability Limit	1.7	7.1	1.4
Laminar Flame Speed (cm/s)	35.5	229.2	7.5
Autoignition Temperature (K)	859	773	930
Minimum Ignition Energy (mJ)	0.280	0.011	8.000
Density (kg/m^3)	0.66	0.08	0.73

Gas turbines are ideal for combined heat and power (CHP) systems because they are long-lasting, require little maintenance, and have little downtime. Their straightforward design and few moving parts enable continuous operation. They also adapt swiftly to load changes and accommodate a variety of fuels, and alter output to match demand, thereby maintaining grid stability and efficiency [10].

Gas turbines serve clean energy goals by employing fuels such as hydrogen and ammonia, which reduce emissions and increase efficiency. They can use a variety of fuels, including high-calorific methane and low-calorific biogas [11]. Their combustion systems can be altered to accept low-octane or hydrogen fuels [12–14].

The LM6000 gas turbine, introduced in 1989, underwent rigorous testing prior to commercial usage. Its superior output and simple-cycle efficiency make it popular in power plants and cogeneration. The CF6-80C2 engine evolved from older GE turbines such as the LM1600, LM2500, and LM5000 [15].

The LM6000 gas turbine supports a variety of fuels, including natural gas, LPG, isopentane, ethanol, diesel, and Coke Oven gas, and allows for rapid switching without shutting down. It ramps at 50 megawatts per minute, which is far quicker than ordinary 5-megawatt turbines. The SPRINT system enhances mass flow and cooling by spray intercooling, with automatic water injection management dependent on the inlet temperature [15].

Since the mid-20th century, hydrogen has been investigated as a fuel for gas turbines. In 1939, Hans von Ohain pioneered its application in these engines. At first hydrogen's combustion qualities appeared promising. However, complications emerged as a result of metal fatigue [16].

Morris [17] studied the effect of hydrogen as a fuel addition in a heavy-duty gas turbine. Hydrogen reduced CO_2 emissions but slightly raised NO_x generation, particularly when injection levels reached up to 10% by volume. Mitsubishi Heavy Industries Ltd. (MHI), Tokyo, Japan, conducted a co-firing experiment with 30% hydrogen by volume in

their new combustor. This technology can reduce CO_2 emissions by around 10% relative to natural gas production [18].

In [19,20], the effect of adding hydrogen on gas turbine efficiency, emissions, and combustion kinetics was assessed by a thermodynamic theory with linked combustion kinetics. The findings revealed that a smaller fuel/air ratio increased efficiency at the largest turbine inlet temperature, resulting in nonlinear variations in emissions and efficiency. The compressor and turbine isentropic efficiencies had the greatest effect on performance, rising with higher levels of hydrogen while also boosting thermal efficiency.

The authors of [21] found that flame sizes reduced with increased hydrogen concentration, resulting in bigger NO_x emissions from higher flame temperatures. However, CO_2 emissions greatly fell.

In May 2020, Kawasaki developed a hydrogen-powered industrial gas turbine using dry low-emission combustion technologies. The system employs micro-mix combustion to attain low NO_x emissions with no water or steam injection, resulting in increased efficiency and lower nitrogen oxide emissions. This method promotes industrial carbon reduction and cleaner energy by allowing high hydrogen fuel utilization, enhancing turbine reliability, and minimizing maintenance [22,23].

In September 2023, Kawasaki launched the world's first hydrogen DLE gas turbine with a micro-mix (MMX) combustor [24]. The M1A-17 platform, with a 1.8 MWe output, allows for cofiring natural gas with 50–100 vol.% hydrogen throughout the entire load band.

As stated by [25], at lower hydrogen concentrations (less than 10%), the flame's combustion characteristics are virtually unaffected. While pure methane increases flame length, adding hydrogen diminishes it. Low levels of hydrogen reduce the lateral mixing zone, resulting in this effect.

In January 2024, Laith Mustafa and Rafał Slefarski analyzed hydrogen/methane mixes in combined cycle gas turbines. They maintained the turbine input temperature at 1723 K to prevent metal burning. The researchers discovered that raising hydrogen content enhanced thermal efficiency and work output. However, when hydrogen passed 20%, NO_x emissions increased dramatically, with pure hydrogen releasing almost three times more NO_x than methane because of higher levels of hydrogen, oxygen, and hydroxyl radicals in the reaction zone [4].

Shih et al. [26] used CFD to examine hydrogen–methane blends in a small gas turbine. They increased hydrogen from 0% to 90% by volume to evaluate flame behavior and emissions. Combustion efficiency remained consistent; however, the combustor design required alterations at high hydrogen levels. In [27], researchers used tests and simulations to investigate pure hydrogen in an improved lean premixed burner. Burners were adjusted to accommodate fluctuating premix levels, and high flow rates hindered flame stabilization in the premix pipe. The results demonstrated that pure hydrogen can be used with emissions under regulatory limits.

Numerous studies concentrate on micro-gas turbines utilizing NH_3 and CH_4 blends. Tohoku University created a micro-gas turbine using ammonia–methane mixes that produced minimal emissions and great thermal performance for small-scale energy production. The research demonstrated the turbine's consistent performance throughout several fuel blends and load conditions [28].

Ślefarski et al. [29] investigated ammonia–methane co-combustion in lean swirl flames with up to 25% ammonia. Modeling with the Eddy Dissipation Concept (EDC) and Reynolds Stress Models (RSMs) revealed that the Okafor mechanism more closely approximated the experimental findings. Heat transfer and volume of the reactor were estimated using CFD, resulting in NO_x emissions within 10% of experimental data. Despite its high computing cost, the 3D RSM simulation is suited for small-scale applications.

In 2022, the Ansaldo AE-T100 micro-gas turbine was examined with ammonia–methane mixes rather than natural gas. Methane was used as a pilot flame, while ammonia levels changed in the main fuel line. The turbine produced 60 kWe at 645 °C and maintained stable operation with up to 63% ammonia. A powerful pilot flame was required for effective ignition [30].

Skabelund et al. [31] investigated ammonia, hydrogen, and methane mixes in a 50 MW Brayton cycle, examining over 5150 fuel combinations. A blend of 78% hydrogen and 22% ammonia reached 44.6% efficiency, which is comparable to methane. Another work designed a micro-gas turbine using partially cracked ammonia in MATLAB/Simulink, exhibiting 74.5–79.1% efficiency and reduced CO_2 emissions [32].

Based on the H-25 series, Mitsubishi Power created a 40 MW gas turbine that runs on ammonia in 2021 [33]. Including a steam cycle will improve efficiency. In comparison to natural gas turbines, ammonia requires a larger combustion chamber because of its slower laminar flame speed.

Experiments demonstrate that increased pressure decreases NO_x emissions in stoichiometric premixed ammonia/air flames. Ammonia produces lower thermal NO_x due to its relatively lower flame temperatures and emits no CO_2 or soot. Additionally its high octane rating offers anti-knock benefits [34]. However, ammonia can still produce large NO_x, causing air pollution [35]. Blending it with fuels like methane can boost combustion speed and lower NO_x emissions, making it more viable as a fuel [36–39].

Due to ammonia's great ignition temperature and smaller flammability range, it requires more safety precautions when being handled, stored, and transported—especially in industrial settings. Hydrocarbon fuels have different combustion characteristics than ammonia. They require more ignition energy and have a slower burning rate of around 7 cm/s, a lower flame temperature, and a smaller flammability range [34,40,41].

Scientists attempted to tackle these challenges. They focused on developing new materials, developing design processes, and studying hydrogen's behavior in turbines. Today, hydrogen continues to be an essential research issue for more environmentally friendly and sustainable energy sources. This research [42] demonstrates that material selection is crucial for the safe and efficient use of ammonia–hydrogen fuels in gas turbines. These fuels have distinct combustion problems, which can result in corrosion, embrittlement, and cracking. High temperatures raise the danger of damage, particularly in turbine blades, necessitating improved materials and analysis methodologies.

Adapting hydrogen and ammonia to use these fuels necessitates significant changes, but it may give viable options that improve safety and infrastructure. This study [43,44] concludes that while hydrogen combustion is sustainably benign, it poses issues in regulating ignition and combustion, potentially leading in knocking. Ammonia is less combustible, requiring engine changes, and produces NO_x emissions that require more treatment.

Oxygen-enriched combustion (OEC) is a promising method for advanced power plants [45]. Replacing nitrogen (N_2) with oxygen (O_2) reduces dilution, increases combustor temperatures, and improves efficiency and capacity [46]. Injecting pure oxygen raises the oxidant's oxygen content [47], enabling more complete combustion and greater energy efficiency.

Oxygen-enriched combustion (OEC) uses less fuel to generate the same power, while lowering pollution and exhaust volume. It supports higher flame temperatures, faster reactions, and greater fuel flexibility, including the use of lower-quality fuels. OEC improves CO_2 capture and enhances combustion control, helping operators optimize performance and adapt to load changes [47,48].

Oxygen-enriched combustion (OEC) enables higher flame temperatures, faster reactions, and greater fuel flexibility, reducing reliance on specific fuels. OEC also en-

hances combustion control, allowing operators to optimize performance and adapt to load changes [47,48].

Although oxy-combustion is well-studied [49–54], OEC lacks experimental data [45]. Bench tests show that oxygen enrichment improves volatile release and reduces burnout temperatures compared to air combustion [55].

A heat flow model [45] shows better combustion and higher flue gas temperatures, increasing boiler efficiency by 2–5% [45]. In fluidized bed combustors, steam injection (steam-to-fuel ratio 0.8) lowers NO_x emissions below 35% oxygen, while 0.5 enhances combustion [55].

While past studies have looked at the effects of H_2, NH_3, and OEC on gas turbines separately, no one has fully explored how these factors work together. The novelty of this study is that it looks at the combined impact of H_2, NH_3, and OEC on gas turbine performance. Using data from GE Gas Power's LM 6000 turbines, this research aims to fill that gap. The main goal is to better understand how these technologies can work together to improve gas turbine efficiency. The research will specifically carry out the following:

(A) Analyze the variation in adiabatic flame temperature with respect to fuel mixture ratio and OEC.
(B) Assess the differences in laminar burning velocity based on fuel mixture ratio and OEC.
(C) Compare thermal efficiency and network output as a function of fuel mixture ratio and OEC.
(D) Perform NO_x emission analysis considering fuel mixture ratio and OEC.

2. Materials and Methods

The methodology used to assess the effects of using hydrogen H_2 and ammonia NH_3 blended with CH_4 as fuels in gas turbine systems, integrating oxygen-enriched combustion (OEC) from the oxidizer stream, is described in this section. It provides thorough explanations of every system, including its elements, information, and underlying assumptions.

Sensitivity analyses were performed on the gas turbine powered by blends of methane–hydrogen and methane–ammonia. Meanwhile, the air's oxygen concentration was varied to examine the effects of both on the gas turbine's NO_x @ 15% O_2 (dry) emissions, burning velocity, thermal efficiency, and adiabatic temperature.

2.1. GE LM6000 Gas Turbine Design and Operating Principle

The operating principle of a gas turbine is to convert fuel into energy utilizing three key components: a compressor, a combustion chamber, and a turbine. The process begins when air is pulled in and compressed, heating it up. This high-pressure air then reacts with fuel and ignites, resulting in the release of superheated gas. As the gas expands, it causes the turbine blades to spin quickly, providing power while keeping the compressor running.

The GE LM6000 gas turbine components are shown in Figure 1. The GE LM6000 is a two-shaft aeroderivative machine built on the CF6-80C2 engine. It is designed for high-performance power generation, offering fast start-up, high efficiency, and fuel diversity. The LM6000 has both low- and high-pressure compressors and turbines. It runs on gas or distillate fuel and minimizes emissions by steam or water injection. The airflow is controlled by three systems: bleed valves, inlet guide vanes, and variable stator vanes.

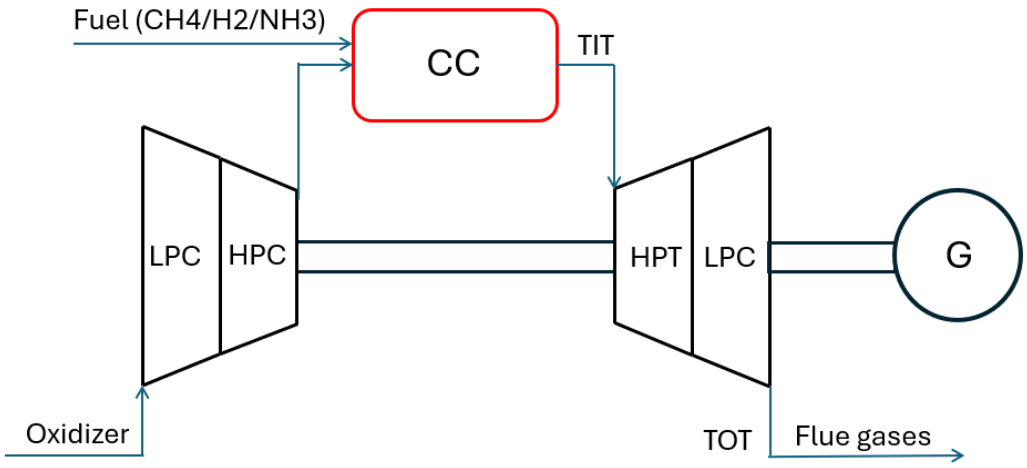

Figure 1. Schematic of GE LM6000 gas turbine [56]. The arrows indicate the flow paths of the oxidizer and fuel blends, whereas the red box represents the combustion chamber (*CC*). *LPC*, *HPC*, *HPT*, and *LPT* refer to the low-pressure compressor, high-pressure compressor, high-pressure turbine, and low-pressure turbine, respectively.

The low-pressure compressor (LPC) module includes a variable inlet guide vane (VIGV) to control incoming airflow, along with LPC stator and rotor assemblies. The LPC is a 5-stage axial-flow compressor based on the LM5000 LPC, which was developed from the CF6-50 booster.

The high-pressure compressor (HPC) is a single-spool, 14-stage axial-flow compressor with variable stator vanes (VSVs) in the inlet guide vane and stages 1 through 5. These vanes help prevent stalls and maintain high efficiency during startup and normal operation [15,56].

There are two available combustion systems: the single annular combustor (SAC) and the dry low-emission (DLE) combustor. The SAC is equipped with 30 externally mounted fuel nozzles and can operate on liquid distillate fuel, natural gas, or both (dual fuel).

The system can also be configured for water or steam injection to reduce NO_x emissions. The DLE combustor has a triple annular design that allows it to run with a uniformly mixed lean fuel–air ratio (premixed mode) throughout the entire power range, helping to minimize emissions [15,56].

The low-pressure turbine (LPT) uses the gas flow from the core of the turbine to drive the low-pressure compressor (LPC) and other connected equipment.

The main parts of the LPT module are a five-stage stator and a five-stage rotor. The LPT rotor powers the LPC and the load either through the midshaft and forward drive adapter (cold-end drive) or directly through the rear drive adapter (hot-end drive).

The high-pressure turbine (HPT) in the LM6000 is a two-stage, air-cooled design that provides high efficiency. It includes the HPT rotor and the Stage 1 and Stage 2 nozzle assemblies. The HPT rotor is mechanically connected to the high-pressure compressor (HPC) and extracts energy from the hot gas stream to drive it. The turbine nozzles guide the hot gas onto the rotor blades at the best angle and speed for maximum performance [15,56].

The accessories connected to the accessory gearbox (AGB) are powered by the high-pressure rotor system. Power is transferred through the inlet gearbox (IGB), a radial drive shaft, and the transfer gearbox (TGB) assembly [15].

In the engine frame and air collector, three structural frames support the bearings for both the low-pressure (LP) and high-pressure (HP) rotors. This frame configuration provides the gas turbine with strong mechanical and dynamic stability and helps control tip clearances for compressor and turbine blades and vanes.

As Table 2 shows, the LM6000 uses three airflow control systems: bleed valves between the LPC and HPC, variable inlet guide vanes (VIGVs) at the LPC inlet, and variable stator vanes (VSVs) in the HPC. These systems enhance compressor stability, prevent stalls, and adjust airflow for different load conditions [15].

Table 2. GE LM6000 specifications [56].

Specification	Details
Turbine Type	Two-shaft aeroderivative machine
Power Generation Output	42.4 MW
Rated Thermal Efficiency	41.4%
Heat Rate	8223 BTU/kWh
Thermal Input	102 MW
Start-up Time	Under 5 min
Rotor Speed (Output Shaft)	3600 rpm
High-Pressure Rotor Speed	6000 to 10,600 rpm
Low-Pressure Compressor (LPC)	5-stage axial-flow
High-Pressure Compressor (HPC)	14-stage axial-flow

2.2. Thermodynamic Analysis

For thermodynamic analysis, this study used Aspen HYSYS, a component-based simulation package specialized in modeling thermodynamic cycles for oil and gas operations, to simulate the power cycle [57]. This program has a complete component library that allows users to pick and set properties for components such as combustion chambers, turbines, and compressors, as well as fuel and oxidizer components.

The program uses energy balances to control fuel behavior and streams to connect them. A component list allows you to specify the material composition of each stream, as well as properties like temperature, pressure, and mass flow. Aspen HYSYS can replicate the steady-state and dynamic performance of complicated chemical/hydrocarbon fluid-based processes by connecting multiple components via material and energy streams.

Air, fuel, and exhaust gas are represented using the Peng–Robinson fluid packages. The combustor was simulated using the GBS Reactor module, which was customized to meet the project's specifications. The combustion chamber and other library components were adapted and programmed to allow new fuel combustion, substituting natural gas or a blend of CH_4/H_2 and CH_4/NH_3. All fuels under consideration were considered to have a constant heat loss from the combustion chamber.

Table 3 shows the input parameters and boundary conditions. It was assumed that the cycle would undergo no mass, heat, or pressure losses.

The mass of oxidizer supplied to the compressor was estimated based on the combustion reaction of the CH_4/NH_3 and CH_4/H_2 blend as indicated in Equation (1) , considering the equivalence ratio changeable to achieve the constant TIT in all situations. Oxygen fraction (x_{O_2}) was chosen to provide the necessary oxidizer for oxygen-enriched combustion (0.21, 0.3, and 0.4). This conclusion was made based on Aspen's component ratio selection and total air mass calculations.

$$m_{OXY} = m_f \cdot \frac{(2g_{CH_4} + 0.5g_{H_2} + 0.75g_{NH_3})\rho_{OXY}}{x_{O_2}\phi} \quad (1)$$

where g_{CH_4}, g_{NH_3} and g_{H_2} denote the mole fraction of CH_4, NH_3 and H_2 in the fuel; in the case of CH_4/H_2, the molar fraction of NH_3 is zero. Conversely, for a CH_4/NH_3 blend, the molar fraction of H_2 is zero, and the density is at standard conditions calculated in Formula (2), where M is the molar mass of components and g is mole fraction of the oxidizer component.

$$\rho_{OXY} = \frac{(g_{N_2} M_{N_2} + g_{O_2} M_{O_2}) p}{RT} \quad (2)$$

Table 3. Input parameters for the GE-LM6000 Aspen HYSYS models [56].

	Unit	Value
Inlet air		
Temperature	K	288
Pressure	MPa	0.1
Fuel		
Pressure	MPa	3.0
Compressor		
PR	-	33
η_{is}	%	85
η_{mech}	%	98.2
Turbine		
P_{out}	MPa	0.1
η_{is}	%	85
η_{mech}	%	98.2
Combustion chamber		
Thermal input	MW	102
Combustion chamber efficiency	-	0.99
TIT	K	1723
Heat losses	kW	0
Pressure losses	%	0

The mass flow rate of fuel was computed for a constant input power of Q_{in} = 102 MW [58], using Formula (3), where g_{CH_4}, g_{NH_3}, and g_{H_2} are the mole fractions of the fuel components, and LHV_{m} is the lower heating value.

$$m_f = \frac{Q_{in}}{(g_{CH_4} \text{LHV}_{m,CH_4} + g_{H_2} \text{LHV}_{m,H_2} + g_{NH_3} \text{LHV}_{m,NH_3})} \quad (3)$$

The thermal efficiency for the GT plant is computed in Equation (4) and the net work by Equation (5).

$$\eta_{\text{th}} = \frac{W_{\text{net}}}{Q_{\text{in}}} \quad (4)$$

$$W_{\text{net}} = W_{\text{turbine}} - W_{\text{compressor}} \quad (5)$$

Figure 2 illustrates the fuel characteristics of methane mixes with ammonia and hydrogen, as well as the impact of CH_4/NH_3 and hydrogen. CH_4/H_2 on the fuel combination's energy characteristics. The higher heating value (HHV) and lower heating value (LHV) rise in proportion to the hydrogen concentration of the CH_4/H_2 mix. The molar masses of CH_4/NH_3 $/H_2$ should be included when determining the LHV and HHV of a gas mixture by volume. This pattern illustrates how hydrogen may significantly raise methane's energy content, making it a desirable option for raising natural gas's calorific value. As the ammonia fraction rises, the LHV and HHV for the CH_4/NH_3 mix fall.

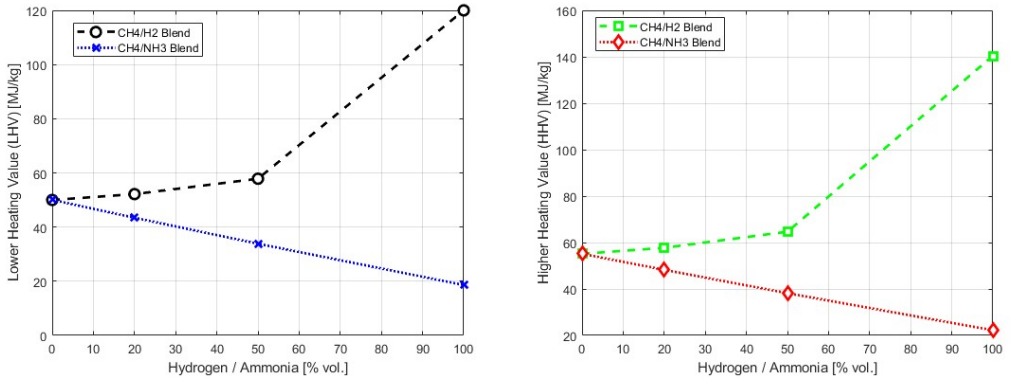

(**a**) (**b**)

Figure 2. (**a**) LHV for CH_4/H_2 and CH_4/NH_3 blends. (**b**) HHV for CH_4/H_2 and CH_4/NH_3 blends.

Figure 3 shows the fuel parameters for blends of CH_4/H_2 and CH_4/NH_3, revealing important trends in the molecular weight (MW) and mass heat capacity of the mixes. Because hydrogen has a much lower molecular weight than methane, the molecular weight of blends including hydrogen drops sharply as the hydrogen proportion increases. The molecular weight (MW) of CH_4/NH_3 has slightly increased. The combination's mass heat capacity increased from 2.44 to 14.21 of pure hydrogen, while there was a minor rise in CH_4/NH_3 mass heat capacity.

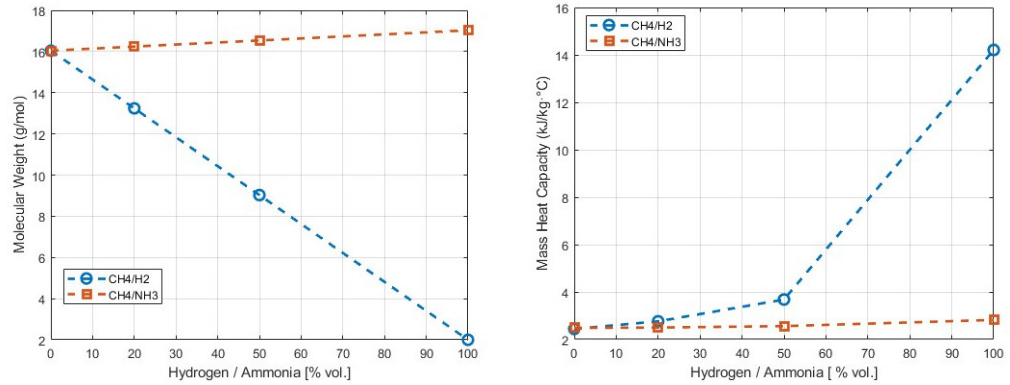

Figure 3. (**Left**) Molecular weight of CH_4/H_2 and CH_4/NH_3 blends. (**Right**) Mass heat capacity of CH_4/H_2 and CH_4/NH_3 blends.

Figure 4 illustrates how methane combines with hydrogen CH_4/H_2 and ammonia CH_4/NH_3 to obtain a thermal input of 102 MW. This indicates major trends in thermodynamic characteristics and fuel efficiency. Adding hydrogen to the CH_4/H_2 combination lowers the mass of fuel required to achieve 102 MW. Because hydrogen has a greater energy content per unit mass than other fuels, the CH_4/NH_3 mix requires more fuel, as ammonia has a lower calorific value than other fuels. Over a variety of hydrogen concentrations, the ratio representing the relationship between specific heat capacities at constant pressure (C_p) and constant volume (C_v) remains relatively constant in the case of CH_4/H_2, and shows a slight increase in the case of CH_4/NH_3.

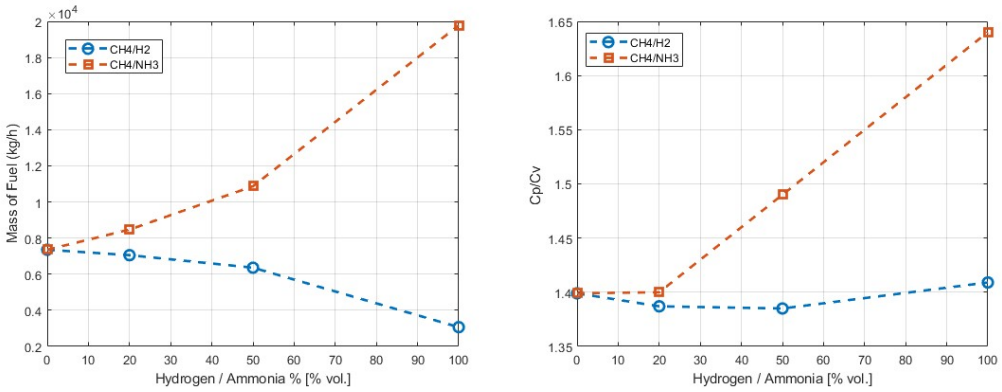

(**a**) (**b**)

Figure 4. (**a**) Mass of fuel of CH_4/H_2 and CH_4/NH_3 blends. (**b**) Specific heat capacities ratio of CH_4/H_2 and CH_4/NH_3 blends.

The model's operation was assumed to be based on the delivery of pressurized hydrogen from water electrolysis and an easily accessible air supply. The Haber–Bosch process then converts green hydrogen into ammonia by mixing it with nitrogen. The ammonia in the gas phase was required to be 65 °C in order to keep the ammonia pressure at 30 bar.

The air was enriched with oxygen generated by water splitting, which results in both hydrogen and oxygen. The air was enriched at three distinct ratios: 21%, 30%, and 40% volume of O_2.

The gas turbine system is made up of three major components, an air compressor (C), a turbine (T), and a combustor (CC), that are connected by a common shaft. The model includes direct combustion, which happens when fuels react with compressed air. The combustion temperature, which is maintained in the combustion chamber at 3.3 MPa, is determined by the oxygen content of the air. A constant-pressure process produces gases at the specified temperature, with a turbine inlet temperature of 1723 K.

The main experiment involved operating a GE LM6000 gas turbine using natural gas fuel with an oxygen enrichment concentration (OEC) of 21%. The simulation results were compared to the turbine's rated performance, focusing specifically on parameters such as net work output and thermal efficiency. The comparison demonstrated that the simulation results closely matched the actual rated performance of the gas turbine, thereby validating the accuracy of the model [56].

The oxygen levels were selected based on [47], and NO_x increases at concentrations above 40 vol.% O_2 due to the generation of additional OH radicals [55].

2.3. Combustion Computation Method

For the calculation of the laminar burning velocity and the adiabatic flame temperature, the software tool of Chemkin was used. To achieve accurate computational predictions and comparisons, the well-validated mechanism of Shrestha et al [59] was used. This was particularly effective in predicting $DME\ /H_2/NH_3/C_xH_y$ mixtures due to their adaptability for predicting premixed flame characteristics. The Shrestha mechanism includes 135 species and 1196 reactions, and this mechanism was updated recently and includes the NO_x chemistry [60].

For the adiabatic flame temperature, a zero-dimensional equilibrium calculation was adopted. Therefore, in the simulations, different volumetric percentages of hydrogen and ammonia were blended into CH_4 as the fuel, using the selected reaction mechanism for the calculation of T_{ad}. The inputs included a range of mixture equivalence ratios (ϕ = 0.33 – 1.0), and an initial temperature of 869 K, while all simulations were carried out

at an initial pressure of 30 bar. These conditions are comparable to the conditions in a turbine combustion chamber.

The one-dimensional freely propagating flame PREMIX code, integrated with the CHEMKIN software, is employed to compute the laminar burning velocity under adiabatic conditions [61]. The combustion domain was adaptively meshed and refined by gradually altering the gradients and curvatures of various output parameters, ensuring that the results are grid-independent.

Detailed reaction mechanisms, reaction kinetics, thermodynamic properties, and transport databases were referenced from various sources. These datasets were interpreted in the solver using thermodynamic and transport data codes [62]. In the simulations, the appropriate reaction mechanism was selected, with different volumetric percentages of hydrogen (0–100%) and ammonia (0–100%), each blended into CH_4 as a fuel, for the same mixture equivalence ratios (ϕ = 0.33–1.0), mole fractions, and initial temperature conditions (869 K) as inputs.

All simulations were again conducted at an initial pressure of 30 bar. Mesh adaptation and refinement criteria, such as GRAD = 0.08 and CURV = 0.05, were applied to the solver. It was observed that the mesh refinement did not affect precision. Thermal diffusion (Soret effect) was included in the computations.

2.4. Combustion Process Modeling

ANSYS Chemkin-Pro 2024 R2 software was used to model the combustion of CH_4/H_2 and CH_4/NH_3 fuels under gas turbine combustion conditions in an oxygen-enriched oxidizer. The modeling employed a Rich–Quench–Lean combustion chamber [4,63] with staged combustion at different equivalence ratios. The combustion system is represented using a chemical reactor network (CRN), consisting of perfectly stirred reactors (PSRs), a plug flow reactor (PFR), and partially stirred reactors (PaSRs), as schematically shown in Figure 5.

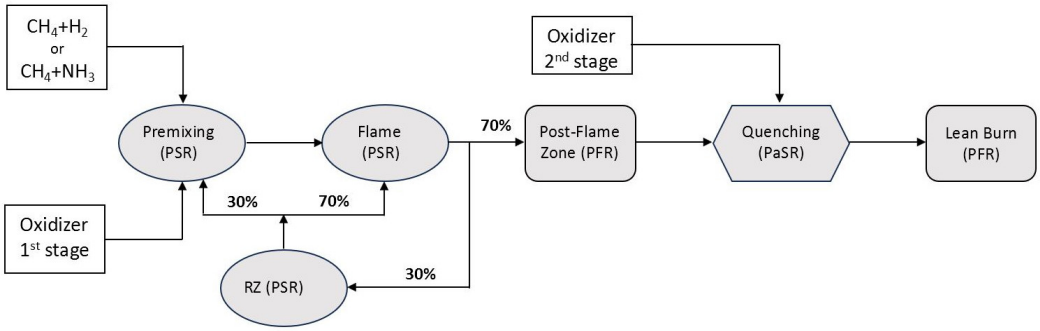

Figure 5. Schematic of the combustion system with a chemical reactor network.

The mixing zone and the internal exhaust gas recirculation zone were modeled using (PSR), with parameters adopted from [64]. The mass of recirculating flue gas, equal to 30% wt. (based on Valera-Medina [65]), was divided into two parts: 70% of the mass of flue gases was delivered to the flame zone, and the remaining portion was directed to the mixing zone.

Reactants from the flame zone fed a flow reactor (PFR) to simulate the reaction in the post-flame zone. The quench/mixing zone was modeled using (PaSR), and the lean combustion zone was modeled with another PFR reactor. The GRI-Mech 3.0 mechanism for CH_4/H_2 (53 species and 325 reactions) [66] and the San Diego mechanism for CH_4/NH_3 fuel with 57 species and 268 reactions [67] were used to model the combustion process and predict the formation of toxic compounds, particularly NO_x.

Tests were conducted for three levels of oxygen in the oxidant: 0.21, 0.3, and 0.4 percent by volume. The remainder of the oxidant was nitrogen. The total amount of oxidant for the tested fuels was varied and adjusted to ensure that the temperature of the flue gas leaving the reactor network was within the range of 1720–1730 K, corresponding to the turbine inlet temperature for the LM6000 turbine.

The air distribution in the RQL sections of the combustion chamber for CH_4/H_2 fuel was chosen based on the literature [68], with ϕ = 1.7 (rich zone, R) and ϕ = 0.5 (lean zone, L). For CH_4/NH_3 fuels, simulations were carried out with varying shares of oxidant supplied to the rich and lean combustion zones, as per [69]: R/L = 10/90, 20/80, and 30/70% of the oxidizer mass. Other parameters for the calculations, obtained from simulations in Aspen HYSYS software, were as follows: input thermal power Q_{in} = 102 MW, oxidizer temperature (primary and secondary) T_{OXY} = 823 K, and combustion chamber pressure P_{CC} = 3 MPa.

While the San Diego mechanism was used for CH_4/NH_3 CRN modeling due to its prior use in the literature, we acknowledge its limitations in capturing NH_2–NO interactions under high-pressure conditions. Future work will consider more advanced NH_3 mechanisms validated for gas turbine applications.

3. Results

This section presents the findings on the impact of blending H_2 and NH_3 with CH_4 on the gas turbine's performance and emissions at different levels of oxygen.

3.1. Global Combustion Properties

Figure 6 shows a comparison of the development of adiabatic flame temperature as a function of equivalence ratio with the addition of hydrogen and the addition of ammonia. Additionally, the dependency on three different oxidizer compositions is investigated.

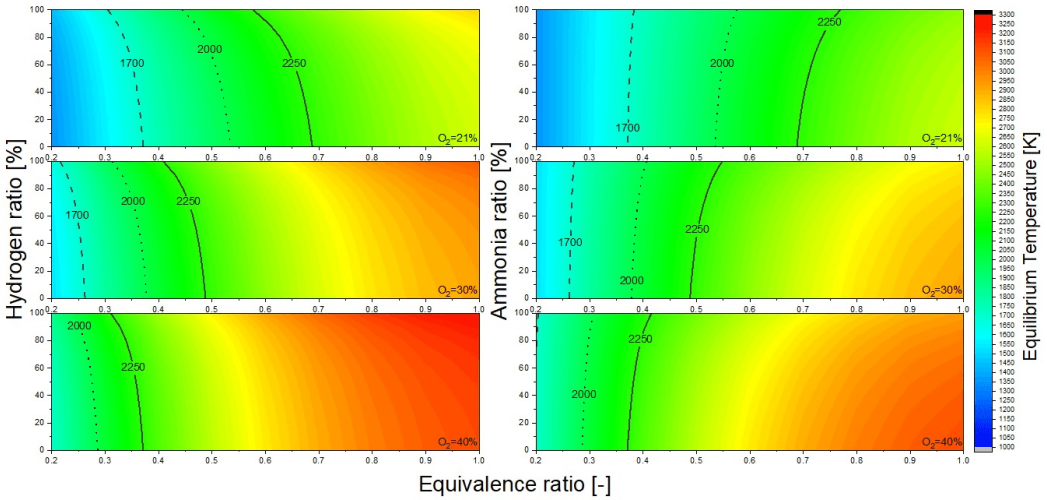

Figure 6. Comparison of the development of adiabatic flame temperature as a function of equivalence ratio with the addition of hydrogen in the **left** column and the addition of ammonia in the **right** column. Additionally, the dependency on three different oxidizer compositions is shown: 21% oxygen at the top, 30% in the middle, and 40% at the bottom, with the remainder being nitrogen. The initial temperature is 869 K and the pressure is 30 bar.

For hydrogen, it can be clearly seen that with an increasing oxygen content, as expected, the temperature rises. It is evident that regardless of the oxygen content, the temperature significantly increases with a higher hydrogen content, displaying a nonlinear trend that shows a marked increase from 60% hydrogen in methane.

For ammonia, it can be demonstrated that temperatures decrease with higher ammonia content. This also occurs nonlinearly but is significantly less pronounced than with hydrogen. Additionally, the temperatures in the ammonia mixtures also rise with an increasing oxygen content in the oxidizer but always remain below those of the hydrogen–methane mixtures.

It is observed that ammonia has no significant impact on temperature with pure air, but as the oxygen content increases, a notable decrease in temperature is evident compared to the natural gas/methane case at the same oxygen content. Considering hydrogen in the discussion, higher hydrogen contents result in increasing temperatures. At 30% oxygen and 100% hydrogen, the temperatures overlap with the case of 40% oxygen and 100% ammonia, with a much higher CO_2 reduction but needing a higher amount of CO_2 separation units; these cases have to be evaluated on the financial side.

In all cases, a nonlinear trend with higher enrichments can be observed, while changes up to 50% fuel switching remain within a range of less than ΔT of 50K for all tested oxygen contents.

In Figure 7, six graphs are presented, displaying laminar burning velocities for hydrogen–methane (left) and methane–ammonia (right) mixtures rather than for temperature, as shown in Figure 6. In the left column, the LBVs of hydrogen–methane mixtures are shown as a function of the equivalence ratio on the x-axis. Additionally, from top to bottom, the graphs represent 21%, 30%, and 40% oxygen in the oxidizer, with the remainder being nitrogen.

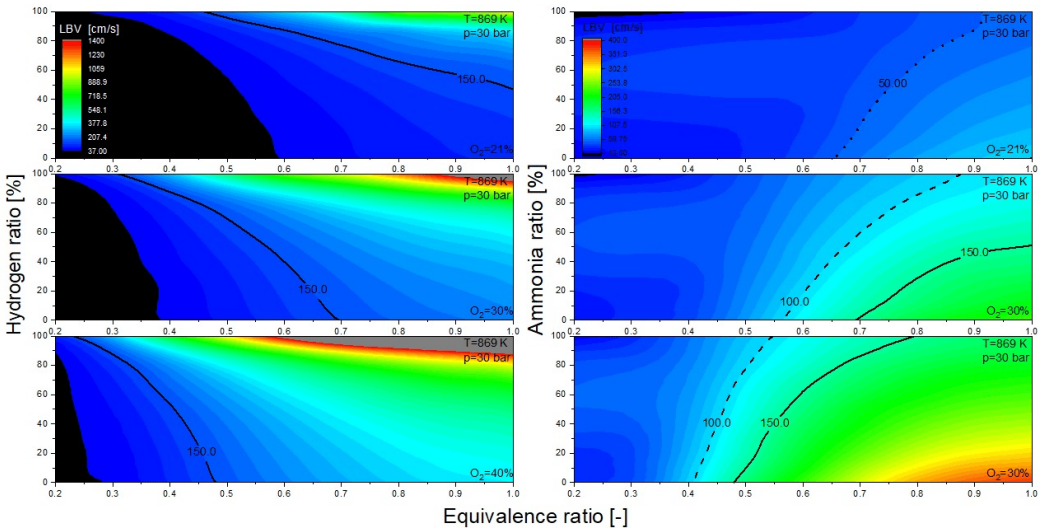

Figure 7. Comparison of the laminar burning velocity as a function of the addition of hydrogen (**left**) and ammonia (**right**). Additionally, the dependency on three different oxidizer compositions is shown: 21% oxygen at the top, 30% in the middle, and 40% at the bottom, with the remainder being nitrogen. The equivalence ratios are ϕ = 0.33–1.0 with an initial temperature of 869 K and a pressure of 30 bar. Note that for clarification, the legend for the top-right graph (21% O_2 for ammonia) is different. All other graphics share the large legend.

The initial temperature was 869 K, and the initial pressure was 30 bar. The results indicate that the LBV significantly increases at higher equivalence ratios near stoichiometry. Moreover, a higher hydrogen content leads to a marked increase in LBV, as corroborated by numerous experiments [70].

In the three graphs, two reference lines are drawn: one at 37 cm/s (the maximum LBV for methane at 1 bar and 298 K) and the other at 270 cm/s (the maximum LBV for hydrogen–air at 1 bar and 298 K). These lines serve as a reference for the shift between

different oxygen levels. If the curves are closely examined, it becomes evident that the addition of hydrogen and ammonia has the opposite effect on the combustion speed.

It is also noteworthy that even with 40% oxygen in the oxidizer, combustion with ammonia only reaches 270 cm/s, which is within the stoichiometric range. As illustrated in Figure 7, the reduction in the presence of ammonia is nearly linear for an equivalence ratio of 0.4 at 30 bar and 869 K.

For 21% and 30%, there is minimal impact compared to the case with 40%, where the reaction rate decreases by approximately 35%. Examining the lower graph for hydrogen, significant changes are observable even at lower equivalence ratios.

The addition of hydrogen markedly increases the burning velocity, exhibiting a non-linear trend. This trend is particularly pronounced at 30% and 40%, leading to a substantial increase starting at 70% hydrogen. In scenarios with 40% oxygen in the oxidizer, the burning velocity increases eight-fold.

3.2. Gas Turbine Operation Analysis

Figure 8 shows a simplified schematic of the modeled gas turbine cycle, with thermodynamic parameters from Table 3. The system employs variable amounts of oxygen-enriched air that enter a compressor with a compression ratio of 33. The air is combusted with a fuel blend of either CH_4/H_2 or CH_4/NH_3 before being delivered to the expander to generate energy for the turbine blades.

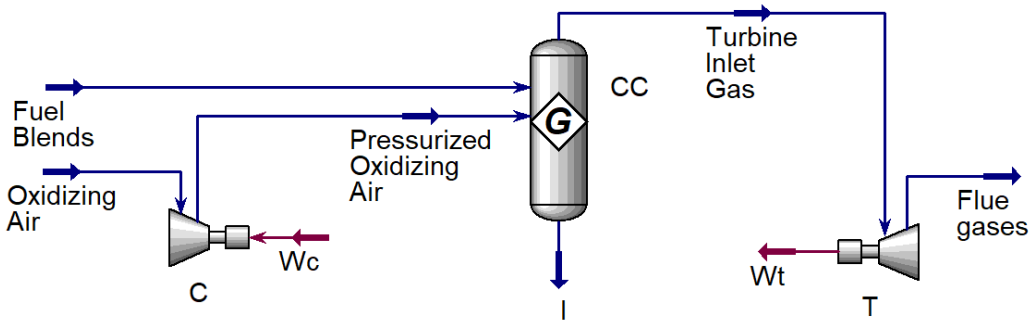

Figure 8. Schematic of a simple gas turbine operating on the Joule–Brayton cycle, simulated in Aspen HYSYS. The system includes a compressor (C) that compresses the oxidizing air using input power (Wc). The pressurized air is then mixed with fuel blends and combusted in the combustion chamber (CC), producing high-temperature gases. These hot gases expand through the turbine (T), generating output power (Wt).

A thermodynamic study on a gas turbine powered by CH_4/H_2 and CH_4/NH_3 mixtures using different oxygen concentrations (21%, 30%, and 40% O_2) highlights the necessity of keeping a constant turbine inlet temperature (TIT) of 1723K to prevent thermal stress that could shorten lifespan. This can be achieved by altering equivalence ratios, as seen in Figures 6 and 9.

The CH_4/H_2 mix's equivalence ratio declines with increasing hydrogen content. For instance, it begins at 0.4 for pure methane with 21% O_2 and falls to approximately 0.35 for pure hydrogen. To reach the necessary TIT, hydrogen requires more oxidizer due to its greater reactivity and LHV. The equivalence ratio decreases with increasing oxygen content, reaching 0.18 for pure hydrogen at 40% O_2, needing more oxidizer for the same TIT.

As ammonia is added to the blend, the equivalence ratio rises due to its lessened reactivity and higher nitrogen concentration. The ratio for 100% ammonia at 21% O_2 is 0.45 (vs. 0.4 for methane). Ammonia produces richer mixtures with lower combustion temperatures. To keep the TIT at 1723 K, the equivalence ratio for pure ammonia at 40% O_2 decreases to 0.24 but stays greater than the CH_4/H_2 blend. Ammonia's lower reactivity

produces richer mixtures, while hydrogen's higher reactivity produces leaner mixtures, which affects combustion stability.

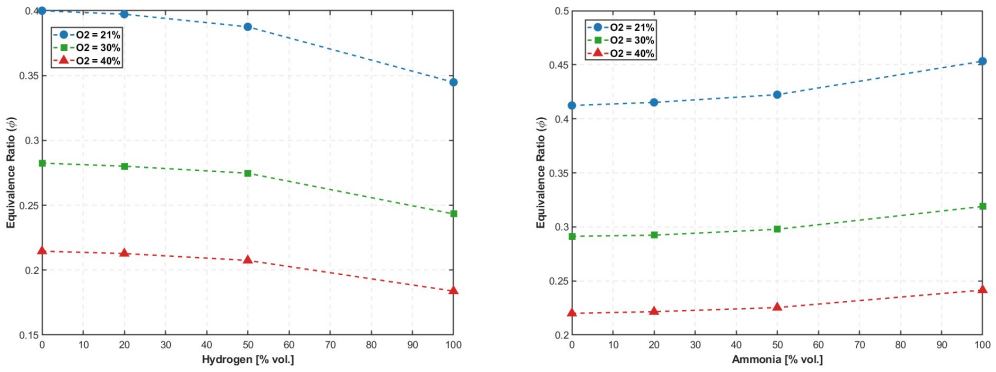

(**a**) (**b**)

Figure 9. (**a**) Equivalence ratio vs. methane/hydrogen fuel blends for different O_2 levels. (**b**) Equivalence ratio vs. methane/ammonia fuel blends for different O_2 levels.

Figure 10 shows how the compressor work (W_C) in a gas turbine system changes with the oxidizer's oxygen level and fuel mixture. In the CH_4/H_2 mix, compressor work reduces as hydrogen content rises because hydrogen has a lower mass. For example, compressor work drops from 51.79 MW for pure methane with 21% oxygen to 50.33 MW for pure hydrogen. As the oxygen amount rises to 30–40%, compressor work decreases, reaching 49.82 MW for pure hydrogen at 30% oxygen and 49.4 MW at 40% oxygen. This indicates a lower oxidizer consumption required to maintain a steady TIT of 1723 K.

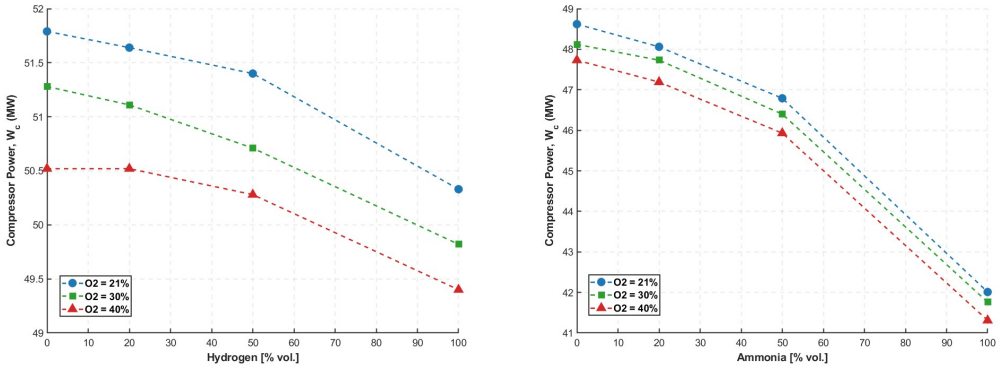

(**a**) (**b**)

Figure 10. (**a**) W_C vs. methane/hydrogen fuel blends for different O_2 levels. (**b**) W_C vs. methane/ammonia fuel blends for different O_2 levels.

The CH_4/NH_3 mix necessitates greater compressor work, especially as the ammonia level increases. For 100% ammonia, compressor work is 42.01 MW. Despite its low heating value, ammonia needs more oxidizer to combust. Compressor work steadily reduces as the oxygen content increases, reaching 41.76 MW at 30% oxygen and 41.31 MW at 40% oxygen for pure ammonia. Oxygen enrichment minimizes compressor effort, but not as much as the CH_4/H_2 blend.

Figure 11 presents turbine work trends for CH_4/H_2 mixes, which are stable but decrease slightly as the amount of hydrogen grows. Hydrogen's increased energy per mass boosts combustion efficiency but also results in lower exhaust temperatures, limiting work extraction. Raising oxygen to 30–40% cuts turbine work a bit, as oxygen improves combustion while decreasing exhaust temperatures and expansion energy.

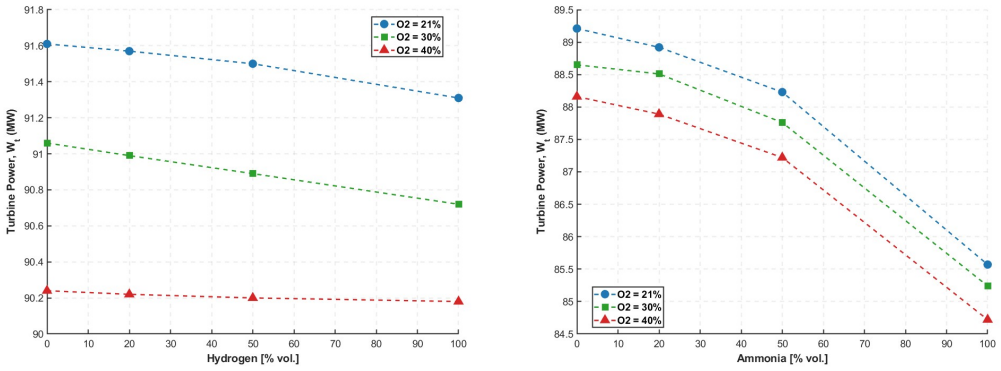

(**a**) (**b**)

Figure 11. (**a**) W_t vs. methane/hydrogen fuel blends O_2 levels. (**b**) W_t vs. methane/ammonia fuel blends for different O_2 levels.

Turbine work falls dramatically in CH_4/NH_3 blends with high ammonia levels. Ammonia's lower calorific value means less power for the turbine, and higher oxygen levels decrease work even more, as ammonia takes more air for burning, lowering exhaust energy and turbine work.

Figure 12 shows how different levels of hydrogen (H_2) and ammonia (NH_3) affect the net work (W_{net}). The W_{net} values for the CH_4/H_2 blend increase as the hydrogen proportion rises, as confirmed by several studies [4,71,72].

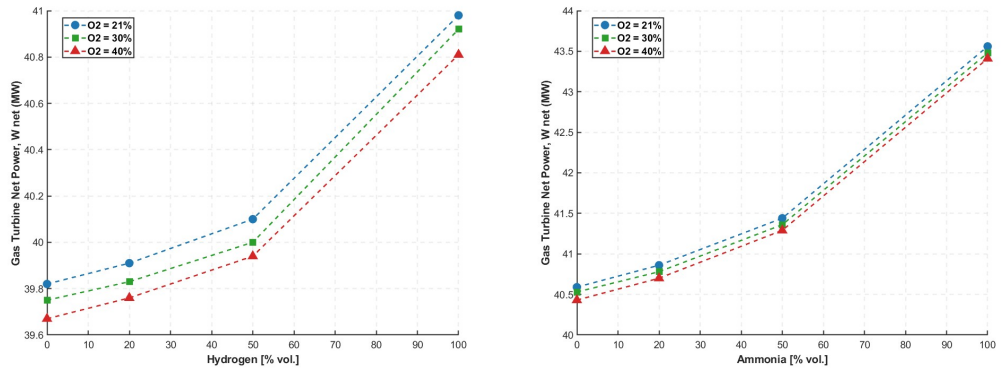

(**a**) (**b**)

Figure 12. (**a**) W_{net} vs. methane/hydrogen fuel blends for different O_2 levels. (**b**) W_{net} vs. methane/ammonia fuel blends for different O_2 levels.

Performance decreases when the air's oxygen content increases because the turbine inlet temperature (TIT) remains constant at 1723 K, which requires reducing the equivalence ratio. The W_{net} values increase slightly from 39.82 MW at 0% H_2 to 40.98 MW at 100% H_2 at 21% O_2, and 40.84 MW at 100% H_2 at 40% O_2. This behavior is due to the higher calorific value and flame temperature caused by the added hydrogen, which improves combustion and increases energy extraction from the fuel, raising Wnet.

The CH_4/NH_3 blend shows higher W_{net} values with more ammonia. The increase is more significant than with the CH_4/H_2 blend, as shown by multiple experiments [31], especially at lower O_2 levels (21%). For the 100% NH_3 blend, Wnet reaches 43.46 MW at 21% O_2. However, as O_2 increases to 30% and 40%, the rise in W_{net} slows down because more oxidizer is needed to maintain the TIT at 1723 K.

Figure 13 shows the thermal efficiency performance of a gas turbine fueled by several fuel mixtures, studied at various hydrogen and ammonia ratios with oxygen-enriched air

at 21%, 30%, and 40%. Increasing the hydrogen component in the CH_4/H_2 mix enhances thermal efficiency due to its larger energy content and better combustion properties. Hydrogen improves combustion by raising both the reaction rate and the flame temperature. Furthermore, lowering the oxygen concentration improves thermal efficiency, with the best efficiency of 40.01% achieved with 21% oxygen-enriched air. This is due to the higher flow rate into the combustion chamber needed to maintain a constant TIT, which improves combustion efficiency and recovery.

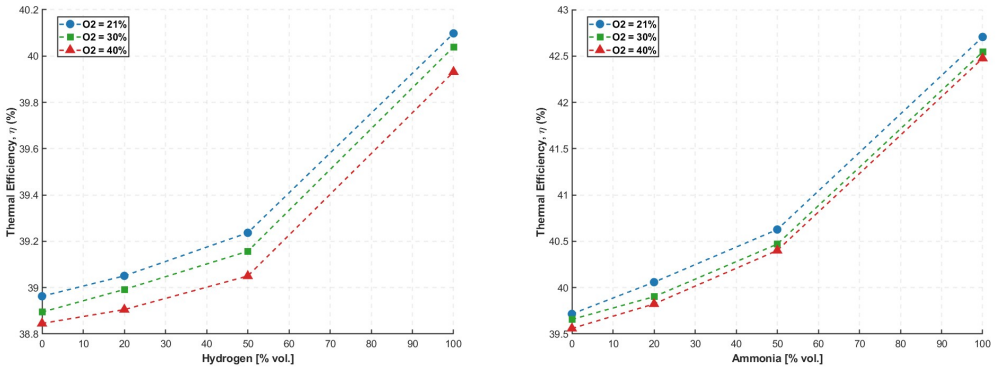

(**a**) (**b**)

Figure 13. (**a**) Thermal efficiency vs. methane/hydrogen fuel blends for different O_2 levels. (**b**) Thermal efficiency vs. methane/ammonia fuel blends for different O_2 levels.

Increasing the ammonia level in the CH_4/NH_3 mixture improves thermal efficiency. The 100% ammonia mixture combined with 21% oxygen-enriched air achieves the best thermal efficiency of 42.7%. Despite its low heating value, ammonia's steady interaction with oxygen results in a more uniform flame structure, which improves the heating system within the turbine.

Adding NH_3 or H_2 to CH_4 reduces flue gas temperature, allowing the turbine to capture additional power from the fuels. Figure 14 demonstrates that increasing the oxygen content in the air greatly increases flue gas temperature, which is supported by [45]. This behavior is crucial for gas turbine operation because flue gas temperature affects thermal load on downstream components, total cycle efficiency, and emission control. The performance metrics for different oxygen levels and fuel blends are shown in Table 4.

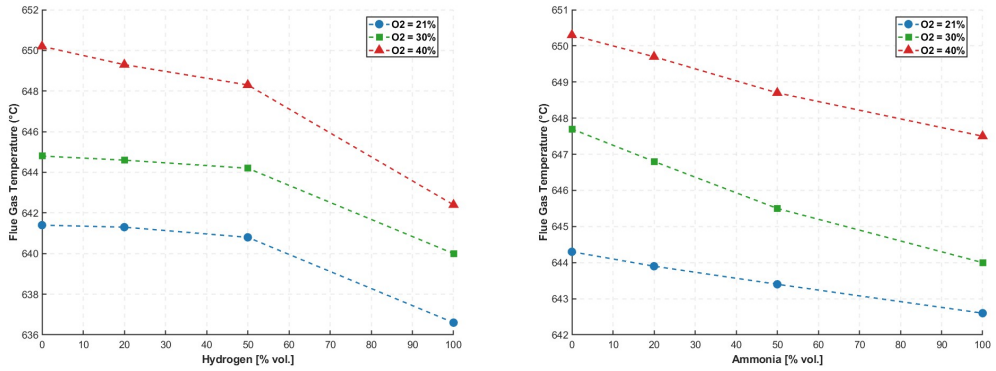

(**a**) (**b**)

Figure 14. (**a**) Flue gas temperature as a function of methane/hydrogen fuel blends for different O_2 levels. (**b**) Flue gas temperature vs. methane/ammonia fuel blends for different O_2 levels.

Table 4. Performance metrics for different oxygen levels and fuel blends.

O_2 (%)	H_2 (% vol.)	W_t (MW)	W_c (MW)	W_{net} (MW)	TOT (K)	η_{th} (%)
21	0	91.61	51.79	39.82	914.55	38.96
21	20	91.55	51.64	39.91	914.45	39.05
21	50	91.50	51.40	40.1	913.95	39.23
21	100	91.31	50.33	40.98	909.75	40.09
30	0	91.03	51.28	39.75	917.95	38.89
30	20	90.96	51.11	39.85	917.75	38.99
30	50	90.80	50.71	40.09	917.35	39.22
30	100	90.74	49.82	40.92	913.15	40.04
40	0	90.24	50.54	39.70	923.35	38.84
40	20	90.23	50.52	39.71	922.15	38.85
40	50	90.22	50.28	39.94	921.45	39.08
40	100	90.21	49.40	40.81	915.55	39.93
O_2 (%)	NH_3 (% vol.)	W_t (MW)	W_c (MW)	W_{net} (MW)	TOT (K)	η_{th} (%)
21	0	89.21	48.62	40.59	917.25	39.71
21	20	88.92	48.06	40.86	916.85	40.05
21	50	88.23	46.9	41.44	916.55	41.00
21	100	85.57	42.01	43.56	915.75	42.70
30	0	88.65	48.12	40.53	920.85	39.73
30	20	88.51	47.73	40.78	918.85	39.98
30	50	87.76	46.40	41.36	918.25	40.06
30	100	85.24	41.76	43.48	917.15	42.62
40	0	88.16	47.73	40.43	923.45	39.63
40	20	87.89	47.19	40.70	922.85	39.90
40	50	87.22	45.93	41.29	922.55	40.48
40	100	84.72	41.31	43.41	920.65	42.55

3.3. Impact of Fuel and Oxidizer Concentrations on NO_x Emissions

3.3.1. Impact of H_2 and Oxidizer Concentration on NO_x Emissions

Figure 15 shows how nitrogen concentration in the oxidizer and hydrogen content in the fuel affect (NO_x) emissions. When it comes to a fuel combination consisting of CH_4/H_2, the thermal process is the main cause of NO_x generation, and temperature is a major factor in determining emission levels.

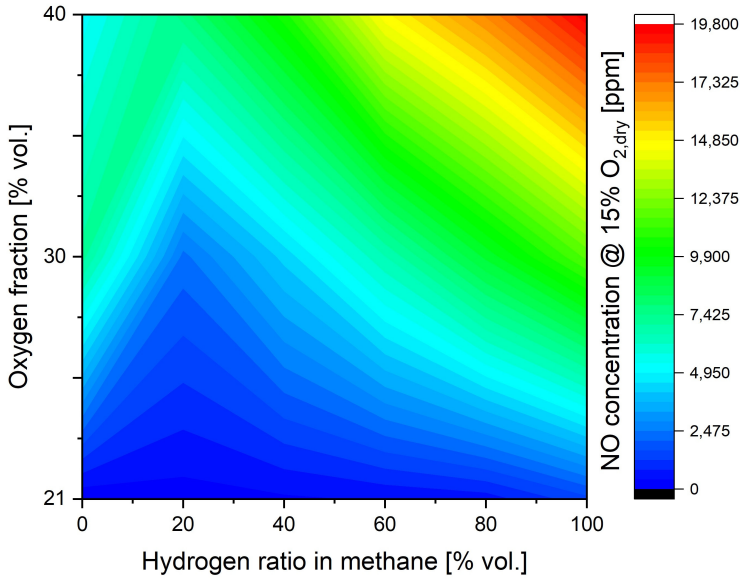

Figure 15. Impact of hydrogen and oxidizer concentration on NO_x emissions.

For all examined oxygen levels, increasing the amount of H_2 in the fuel while keeping the equivalence ratio ϕ constant in the rich combustion zone raises the combustion temperature by about 300 K for $x_{H_2} = 100\%$ vol. NO_x emissions for O_2 = 21% vol. due to this temperature increase multiple-fold, from 65 ppm at $x_{H_2} = 0\%$ vol. to 951 ppm at $x_{H_2} = 100\%$ vol. However, O_2 = 40% vol. and pure hydrogen were found to have the greatest emissions, coming in at 19,705 ppm. The combustion temperature of this fuel mixture is more than 600 K higher than that of CH_4 oxidized in O_2 = 21% vol.

The increase in combustion temperature with higher O_2 results from the reduced mass flow of combustion products due to a lower nitrogen content in the oxidizer. The rise in NO_x emissions is further amplified by the increased concentration of oxygen radicals (O) in the flame, which promotes the reaction. The relation between NO_x emissions and the equivalence ratio is shown in Table 5.

$$\mathrm{O} + \mathrm{N_2} \rightarrow \mathrm{NO} + \mathrm{N} \tag{6}$$

Table 5. NO_x emissions [ppm] and equivalence ratio at various H_2 concentrations and oxidizer levels.

H_2 % vol.	**21% O_2**		**30% O_2**		**40% O_2**	
	NO_x	ϕ	NO_x	ϕ	NO_x	ϕ
0	65	0.40	7194	0.283	5150	0.21
20	218	0.39	2341	0.28	7620	0.206
40	342	0.38	4271	0.27	10,563	0.204
60	470	0.37	6588	0.26	14,726	0.2
80	607	0.36	9193	0.25	16,999	0.19
100	1519	0.35	11,674	0.24	19,705	0.18

3.3.2. Impact of NH_3 and Oxidizer Concentration on NO_x Emissions

The RQL2 combustion chamber model was used to numerically simulate the combustion process for CH_4/NH_3 mixtures in oxidizers with 21%, 30%, and 40% oxygen. The rich combustion zone (R) and the lean combustion zone (L) are the two separate zones that make up this sort of chamber.

The exhaust gas temperature was kept between 1720 and 1730 K by adjusting the total amount of air delivered to the chamber. Three distinct oxidizer mass fractions (R = 10 wt.%, 20 wt.%, and 30 wt.%) were given to the rich zone in the simulations, while the remaining air was routed to the lean zone. Figures 16–18 show the outcomes of various simulations.

Two main mechanisms contribute to the generation of (NO_x) during the combustion of CH_4/NH_3 mixes: the fuel-bound mechanism, which is driven by ammonia oxidation based on the reaction Formula (7) , and the thermal mechanism, which is dominant for mixtures with low ammonia concentrations.

$$\mathrm{NH_3} + 1.25\,\mathrm{O_2} \rightarrow \mathrm{NO} + 1.5\,\mathrm{H_2O} \tag{7}$$

One essential element that makes this pathway possible is the presence of oxygen in the reaction zone. An examination of the simulation findings under O_2 = 21% vol. and O_2 = 30% vol. conditions showed that when the fuel's NH_3 concentration increases, NO_x emissions first rise before starting to fall.

The NO_x emission curve's inflection point was determined to be influenced by the oxidizer's composition as well as the oxidizer mass fraction (R) added to the rich combustion zone. The maximum combustion temperatures for oxidizers with O_2 = 21% and O_2 = 30% are limited to 1600 K and 2200 K, respectively, when only 10 weight percent of the oxidizer is supplied to the R zone. In these circumstances, the rich zone's restricted oxygen availability prevents the creation of fuel-bound and thermal NO_x. The subsequent

oxidizer delivery to the lean zone (L) causes NO_x production in the quenching (PaSR reactor) and lean burn zones. At higher oxidizer mass fractions (R = 20 wt.% and 30 wt.%) and O_2 levels of 21% and 30%, NO_x generation occurs in the post-flame zone, driven by the thermal process, with simultaneous NO_x reduction via reactions involving NHi and OH radicals. Similar behavior is found for O_2 = 21% and R = 30 wt.%. Injecting oxidizer into the quenching and lean burn zones, represented by the PASR and PSR reactors, leads to the rapid oxidation of NH_3 to NO_x. In fuel mixtures containing 80–100% vol. NH_3, this oxidation pathway occurs concurrently with partial NO_x reduction through radical species created by ammonia breakdown.

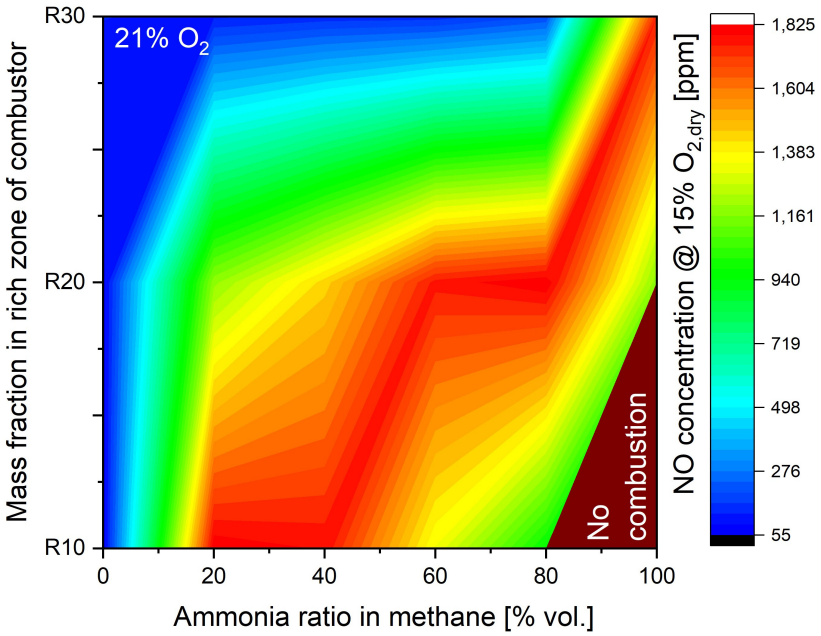

Figure 16. NO_x emissions for CH_4/NH_3 fuel under O_2 = 21%.

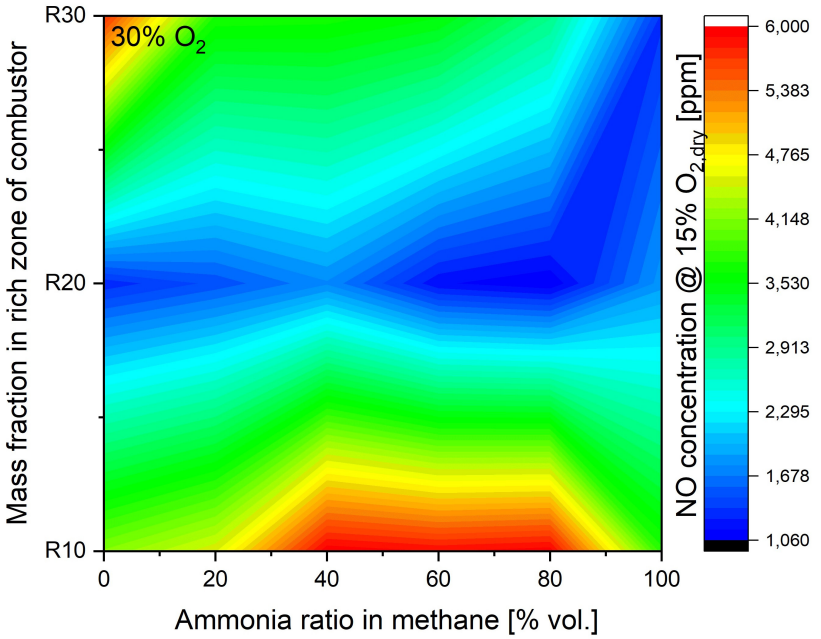

Figure 17. NO_x emissions for CH_4/NH_3 fuel under O_2 = 30%.

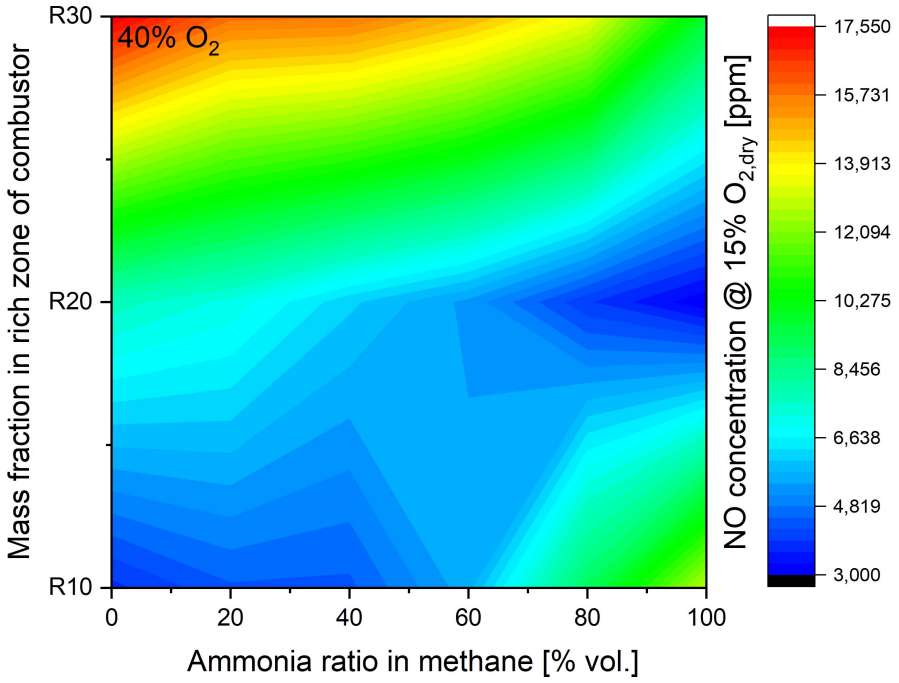

Figure 18. NO_xemissions for CH_4/NH_3 fuel under O_2 = 40%.

The distribution of the oxidizer has a major effect on the trend in NO_x emissions, with O_2 = 40% vol. Rising NO_x emissions are caused by raising the NH_3/CH_4 ratio at low oxygen availability in the reaction zone (R = 10 wt.%). In contrast, the reverse trend is seen for R = 20 wt.% and 30 wt.%, when NO_x emissions fall as the ammonia content rises.

In situations when O_2 = 40% and R values are 10, 20, and 30 wt.%, as well as when O_2 = 30% and R = 30 wt.%, the oxygen supply in the rich zone is sufficient to ensure that the fuel is completely oxidized. This causes combustion temperatures to rise over 2300 K and possibly as high as 2900 K (for O_2 = 40% and R = 30 wt.%). Significant NO_x generation is facilitated by these high temperatures by both fuel-bound and thermal processes, and NO_x concentrations at the R zone exit surpass several thousand ppmv. Reactive radicals (O, H, OH, and NH_i) are also found in considerable amounts at the R zone outlet.

When the flue gas is diluted with an oxidizer, the temperature drops, which promotes the reduction of NO_x through reactions involving NH_i radicals, such as:

$$\mathrm{NO} + \mathrm{NH_2} \rightleftharpoons \mathrm{N_2} + \mathrm{H_2O}. \quad (8)$$

The combustion analyses of CH_4/NH_3 blends in RQL and RQL2 chambers designed for low-calorific fuels, using CRN models, indicate that modifications to current combustion systems are necessary for the practical implementation of ammonia as a fuel. One approach explored in the literature [73] involves the preliminary thermal or catalytic cracking of NH_3 into H_2 and N_2, followed by the oxidation of the resulting $CH_4/NH_3/H_2$ mixture. Table 6 shows NO_x emissions at various NH_3 concentrations, oxidizer levels, and rich zone mass fractions.

The production of intermediate radicals like NH_2 and NH becomes important at high NH_3 concentrations, especially in fuel-rich or staged combustion settings. These radicals take part in processes that reduce NO, particularly by competing with thermal NO generation. This chemical pathway lowers NO emissions overall. This change in the major response pathways is reflected in the inflection behavior shown in the simulated findings. These results align with earlier kinetic and experimental investigations of ammonia combustion [73].

Table 6. NO_x emissions at various NH_3 concentrations, oxidizer levels, and rich zone mass fractions.

NH_3 % vol.	21% O_2			30% O_2			40% O_2		
R %wt.	10	20	30	10	20	30	10	20	30
0	59	70	130	4165	1302	5745	3802	7706	17,535
20	1819	1187	121	4543	1503	3722	4463	7143	15,858
40	1784	1437	142	5988	1763	3694	4432	6107	15,780
60	1342	1767	145	5892	1182	3550	5618	5329	14,844
80	965	1821	203	5967	1069	2937	9144	3956	13,554
100	No Combustion	1175	1752	3775	1838	1342	12,778	3049	9762

4. Discussion

4.1. Material Compatibility Challenges

While this study demonstrates the thermodynamic benefits of hydrogen and ammonia blends under oxygen-enriched combustion, practical implementation faces material compatibility challenges.

Hydrogen embrittlement (HE) is a critical failure mechanism in high-strength metals, which are often used in gas turbines. In HE, hydrogen atoms diffuse into the material and degrade its mechanical properties, notably the ductility and fracture toughness. This degradation is driven by several key mechanisms [42,74].

One is internal pressure, in which hydrogen atoms recombine into H_2 molecules within microvoids, generating internal stresses that can lead to cracking or surface blistering. Due to the fueling situation in turbines, this mechanism could be more strongly promoted than in other combustion systems [42].

Another mechanism is hydrogen-enhanced decohesion (HEDE), where hydrogen reduces the strength of atomic bonds, especially at stress concentrators, resulting in brittle fracture. Additionally, hydrogen-enhanced localized plasticity (HELP) increases dislocation mobility at crack tips, allowing cracks to propagate even under relatively low stress. Environments rich in hydrogen sulfide H_2S, hydrochloric acid (HCl), or moisture significantly exacerbate HE. This phenomenon is particularly dangerous in the aerospace and energy sectors, where sudden, unpredictable failure of structural components can occur under operational loads [42].

When employing hydrogen in combustion, the system may need to be modified in order to prevent the deterioration of turbine performance. These modifications could include altering the mass flow rate, the pressure ratio, or the cycle's design and structure [74].

Similarly, ammonia-induced corrosion poses a major challenge, particularly for brass and copper alloys. These materials are prone to stress corrosion cracking (SCC) in the presence of ammonia. A key issue is dezincification, where zinc is selectively leached in aqueous ammonia, leaving behind a porous, high-stress, copper-rich layer that is more susceptible to cracking. These degradation mechanisms underscore the limitations of conventional materials in aggressive environments [75,76].

In response, high-entropy alloys (HEAs)—engineered from elements like Ni, Fe, Cr, Co, and Mo—are emerging as advanced alternatives. Their high entropy of mixing helps resist localized corrosion phenomena such as pitting and crevice corrosion, even in seawater or ammonia exposure [75].

HEAs also offer practical benefits; their high iron content helps reduce manufacturing costs, while their superior corrosion resistance and durability extend service life in extreme applications such as offshore platforms and ammonia processing facilities. By addressing both hydrogen embrittlement and chemical corrosion, HEAs represent a promising material solution for next-generation structural performance [75].

Thermal barrier coatings (TBCs), which shield turbine blades from extreme heat, can be harmed by hydrogen and ammonia. It is possible that yttria-stabilized zirconia (YSZ), a common TBC, is unable to manage these fuels [77].

4.2. Model Limitations

This study uses steady-state simulations with several simplifications. Ideal gas properties were assumed, and combustion was modeled using a simplified CRN approach. Transient behavior, blade cooling, and pressure losses were not included. These assumptions help focus on comparative trends but introduce uncertainties that should be considered when interpreting the results.

This study uses a chemical reactor network (CRN) with PSR, PFR, and PaSR elements to compare different fuel blends and oxygen enrichment levels. While this approach allowed for consistent comparisons, it simplifies the complex combustor flow field and does not capture key turbulence–chemistry interactions, especially in Rich–Quench–Lean (RQL) combustion with ammonia fuels.

This means factors like recirculation zones and localized flame dynamics, which affect NO_x emissions, are not fully captured. We suggest that future work use CFD modeling or reactor sensitivity studies to better understand how reactor configuration impacts emissions.

It is important to note that despite the increase in oxygen concentration, the laminar burning velocity of NH_3 remains relatively low. This presents practical challenges for ignition and flame stabilization. In real-world applications, ignition of NH_3-based mixtures typically requires a pilot flame, high-energy ignition system, or the addition of more reactive fuels such as hydrogen or methane. These considerations are essential for the practical deployment of NH_3 as a gas turbine fuel.

4.3. Radical Effects and NO_x Chemistry

When the hydrogen level exceeds 60%, the flame temperature increases sharply and nonlinearly. This can be attributed to the combustion chemistry. In hydrogen-rich mixtures, the reaction

$$\mathrm{H} + \mathrm{O_2} \rightarrow \mathrm{OH} + \mathrm{O} \tag{9}$$

becomes increasingly dominating. This chain-branching stage generates OH and O radicals, which are highly reactive and speed up the combustion process. As a result, more heat is emitted over a shorter period of time, causing a notable flame temperature increase. This trend reflects hydrogen's heightened reactivity at high concentrations, as well as the crucial role of radical generation in driving combustion dynamics.

The reduction in NO_x emissions observed in ammonia-rich blends, especially under oxygen-enriched conditions, reflects the complex chemistry of NO_x formation and destruction. While NO_x is typically produced through thermal, prompt, and fuel-based mechanisms, the behavior changes as the ammonia concentration increases. Under these conditions, reactions that consume NO become more prominent. One important example is the interaction between NH_2 radicals and NO, which forms nitrogen and water.

$$\mathrm{NH_2} + \mathrm{NO} \rightarrow \mathrm{N_2} + \mathrm{H_2O} \tag{10}$$

This shift helps explain the lower NO levels we observed. Although we did not carry out a detailed reaction path or sensitivity analysis in this study, the results suggest that NO-reducing reactions play a growing role at higher NH_3 concentrations. This warrants further exploration in subsequent work.

4.4. Comparison of Chemical Kinetic Mechanisms

In this study, three chemical kinetic mechanisms—Shrestha, GRI-Mech 3.0, and San Diego—were considered for modeling combustion characteristics of CH_4 blended with H_2 or NH_3. Table 7 summarizes the key differences among these mechanisms for flame temperature and NO_x emission prediction.

Table 7. Comparison of chemical kinetic mechanisms for flame temperature and NO_x emission prediction.

Property	Shrestha	GRI-Mech 3.0	San Diego
Species	135	53	57
Reactions	1196	325	268
Validation Scope	$H_2/NH_3/CH_4$	CH_4/H_2	CH_4/NH_3
Flame Temperature	High accuracy	Moderate accuracy	Moderate to high
NO_x Emissions	Moderate accuracy	High accuracy	Moderate to high

4.5. Trade-Off Between Efficiency Gains and NO_x Emissions

Although the increase in net power output is modest (1–3 MW), the use of hydrogen or ammonia offers significant environmental benefits by eliminating CO_2 emissions; however, the corresponding rise in NO_x emissions—especially under oxygen-enriched conditions—necessitates the integration of emission control strategies. Practical deployment would require a careful balance between efficiency gains and environmental impact, considering both regulatory constraints and the cost of mitigation technologies.

5. Conclusions

This research assessed the performance of a GE LM6000 gas turbine using two fuel blends of methane/hydrogen and methane/ammonia at varying oxygen levels (21%, 30%, and 40% O_2).

The turbine ran at a constant temperature of 1723 K (TIT) with a heat input of 102 MW. Increasing hydrogen content, especially above 60%, leads to a nonlinear rise in adiabatic flame temperature, a trend further amplified by oxygen enrichment. In contrast, adding ammonia decreases flame temperature despite the elevated oxygen levels. Laminar burning velocity (LBV) increased significantly with higher hydrogen fractions (up to eight-fold at 100% H_2 and 40% O_2), whereas ammonia addition reduced LBV, particularly under oxygen-rich conditions.

To maintain constant turbine temperature, the equivalence ratio reduced as hydrogen concentration increased, especially at 40% O_2. Hydrogen-rich blends required leaner mixtures ($\phi = 0.18$ at 100% H_2, 40% O_2), while ammonia-rich blends required richer mixtures ($\phi = 0.45$ at 100% NH_3, 21% O_2).

There was an increase in power output from 39.82 MW to 40.98 MW, with a maximum efficiency of 40.01% at 100% hydrogen and 21% oxygen. Pure ammonia had the highest power production (43.46 MW) and efficiency (42.7%) at 21% O_2. However, performance increases dropped with increased oxygen levels.

CH_4/H_2 blends had increased NO_x emissions, particularly at higher hydrogen and oxygen levels. The maximum NO_x emissions occurred at 40% O_2 and 100% hydrogen, reaching 19,705 ppm. In contrast, CH_4/NH_3 blends yielded lower NO_x emissions, and increased ammonia concentration further reduced them. Proper oxidizer control also contributed to reduced emissions.

While this study provides useful information, it has limitations, including the lack of experimental validation and detailed CFD simulations. As gas turbine testing requires substantial funding and industrial collaboration, such validation is beyond the current

scope. Future research should therefore focus on securing collaborative funding to enable experimental testing and high-fidelity simulations (e.g., GT-Suite, GasTurb), alongside developing effective NO_x reduction strategies such as advanced combustion techniques and SCR technologies.

Author Contributions: Conceptualization, L.M., R.Ś., R.J. and S.E.; methodology, L.M., R.Ś., R.J. and S.E.; software, L.M., R.Ś., R.J. and S.E.; validation, L.M., R.Ś., R.J., M.A. and S.E.; formal analysis, L.M. and R.Ś.; investigation, L.M. and R.Ś.; resources, L.M., R.Ś., R.J., M.A. and S.E.; data curation, L.M., R.Ś., R.J., M.A. and S.E.; writing—original draft preparation, L.M.; writing—review and editing, L.M., R.Ś. and S.E.; visualization, L.M., R.Ś., R.J., M.A. and S.E.; supervision, L.M., R.Ś., R.J., M.A. and S.E.; project administration, L.M. and R.Ś. All authors have read and agreed to the published version of the manuscript.

Funding: This research received no external funding.

Institutional Review Board Statement: Not applicable.

Informed Consent Statement: Not applicable.

Data Availability Statement: The data are available on request from the corresponding author for reasonable reasons.

Conflicts of Interest: The authors declare no conflicts of interest.

Abbreviations

The following abbreviations are used in this manuscript:

A/F	Air to Fuel Ratio
C	Compressor
CC	Combustion Chamber
CHP	Combined Heat And Power
Cp	Specific Heat At Constant Pressure
CRN	Chemical Reactor Network
F_g	Flue Gas
GT	Gas Turbine
GTs	Gas Turbine Systems
HHV	Higher Heating Value
LBV	Laminar Burning Velocity
LHV	Lower Heating Value
M	Molar Mass
NG	Natural Gas
NO_x	Nitrogen Oxide
OEC	Oxygen-Enriched Combustion
OXY	Oxidizer
p	Pressure
PaSR	Partially Stirred Reactor
PFR	Plug Flow Reactor
PR	Pressure Ratio
PSR	Perfectly Stirred Reactor
Q_{in}	Input Power
R	Gas Constant, 8.314 J/mol·K
RQL	Rich–Quench–Lean Combustor
RZ	Recirculation Zone
T	Temperature
TIT	Turbine Inlet Temperature
TOT	Turbine Outlet Temperature

W_c	Compressor Power
W_{net}	Gas Turbine System Power
W_t	Turbine Power
ϕ	Equivalence Ratio
η	Efficiency
η_{is}	Isentropic Efficiency
η_{mech}	Mechanical Efficiency
η_{th}	Thermal Efficiency
γ	Heat Capacity Ratio
ρ	Density

References

1. Arora, P. COP28: Ambitions, realities, and future. In *Environmental Sustainability*; Springer: Berlin/Heidelberg, Germany, 2024; Volume 13, pp. 1–7.
2. Nevitt, M. Assessing COP28: The New Global Climate Deal in Dubai. Just Security. 2023. Available online: https://www.justsecurity.org/90710/assessing-cop-28-the-new-global-climate-deal-in-dubai/ (accessed on 7 May 2025) .
3. Babaremu, K.; Olumba, N.; Chris-Okoro, I.; Chuckwuma, K.; Jen, T.C.; Oladijo, O.; Akinlabi, E. Overview of solar–wind hybrid products: Prominent challenges and possible solutions. *Energies* **2022**, *15*, 6014. [CrossRef]
4. Mustafa, L.; Ślefarski, R.; Jankowski, R. Thermodynamic Analysis of Gas Turbine Systems Fueled by a CH_4/H_2 Mixture. *Sustainability* **2024**, *16*, 531. [CrossRef]
5. Kumar, S.S.; Lim, H. An overview of water electrolysis technologies for green hydrogen production. *Energy Rep.* **2022**, *8*, 13793–13813. [CrossRef]
6. Ni, M.; Leung, M.K.; Leung, D.Y. Technological development of hydrogen production by solid oxide electrolyzer cell (SOEC). *Int. J. Hydrog. Energy* **2008**, *33*, 2337–2354. [CrossRef]
7. The Royal Society. *Ammonia: Zero-Carbon Fertiliser, Fuel and Energy Store*; Policy Briefing, DES5711; The Royal Society: London, UK, 2020; ISBN 978-1-78252-448-9.
8. Aziz, M.; Wijayanta, A.T.; Nandiyanto, A.B.D. Ammonia as effective hydrogen storage: A review on production, storage and utilization. *Energies* **2020**, *13*, 3062. [CrossRef]
9. Valera-Medina, A.; Xiao, H.; Owen-Jones, M.; David, W.I.; Bowen, P. Ammonia for power. *Prog. Energy Combust. Sci.* **2018**, *69*, 63–102. [CrossRef]
10. Poullikkas, A. An overview of current and future sustainable gas turbine technologies. *Renew. Sustain. Energy Rev.* **2005**, *9*, 409–443. [CrossRef]
11. Valera-Medina, A.; Banares-Alcantara, R. *Techno-Economic Challenges of Green Ammonia as an Energy Vector*; Academic Press: Cambridge, MA, USA, 2020.
12. Lammel, O.; Schütz, H.; Schmitz, G.; Lückerath, R.; Stöhr, M.; Noll, B.; Aigner, M.; Hase, M.; Krebs, W. FLOX® combustion at high power density and high flame temperatures. *J. Eng. Gas Turbines Power* **2010**, *132*, 121503. [CrossRef]
13. Zornek, T.; Monz, T.; Aigner, M. Performance analysis of the micro gas turbine Turbec T100 with a new FLOX-combustion system for low calorific fuels. *Appl. Energy* **2015**, *159*, 276–284. [CrossRef]
14. Lückerath, R.; Meier, W.; Aigner, M. FLOX® combustion at high pressure with different fuel compositions. In Proceedings of the ASME Turbo Expo 2007: Power for Land, Sea, and Air, Montreal, QC, Canada, 14–17 May 2007 .
15. Badeer, G. *GE Aeroderivative Gas Turbines-Design and Operating Features;* GER-3695E; GE Power Systems: Evendale, OH, USA, 2000.
16. Langston, L.S. Hydrogen fueled gas turbines. *Mech. Eng.* **2019**, *141*, 52–54. [CrossRef]
17. Morris, J.D.; Symonds, R.A.; Ballard, F.L.; Banti, A. *Combustion Aspects of Application of Hydrogen and Natural Gas Fuel Mixtures to MS9001E DLN-1 Gas Turbines at Elsta Plant, Terneuzen, The Netherlands*; American Society of Mechanical Engineers: New York, NY, USA, 1998; Volume 78644.
18. Inoue, K.; Miyamoto, K.; Domen, S.; Tamura, I.; Kawakami, T.; Tanimura, S. Development of hydrogen and natural gas co-firing gas turbine. *Mitsubishi Heavy Ind. Tech. Rev.* **2018**, *55*, 1.
19. Skabelund, B.B.; Jenkins, C.D.; Stechel, E.B.; Milcarek, R.J. Thermodynamic and emission analysis of a hydrogen/methane fueled gas turbine. *Energy Convers. Manag. X* **2023**, *19*, 100394. [CrossRef]
20. Imteyaz, B.A.; Nemitallah, M.A.; Abdelhafez, A.A.; Habib, M.A. Combustion behavior and stability map of hydrogen-enriched oxy-methane premixed flames in a model gas turbine combustor. *Int. J. Hydrog. Energy* **2018**, *43*, 16652–16666. [CrossRef]
21. Rajpara, P.; Shah, R.; Banerjee, J. Effect of hydrogen addition on combustion and emission characteristics of methane fuelled upward swirl can combustor. *Int. J. Hydrog. Energy* **2018**, *43*, 17505–17519. [CrossRef]

22. Horikawa, A.; Okada, K.; Wirsum, M.; Funke, H.H.W.; Kusterer, K. 100% hydrogen dry low NOx combustor developments for 2MW class gas turbine. In Proceedings of the International Conference on Power Engineering (ICOPE) 2021, Virtual, 17–21 October 2021; The Japan Society of Mechanical Engineers: Tokyo, Japan, 2021.
23. Funke, H.H.W.; Beckmann, N.; Keinz, J.; Horikawa, A. 30 years of dry-low-Nox micromix combustor research for hydrogen-rich fuels—An overview of past and present activities. *J. Eng. Gas Turbines Power* **2021**, *143*, 071002. [CrossRef]
24. Kroniger, D.; Kamiya, H.; Horikawa, A.; Suzuki, R.; Munktell, E.; Braun, R. LES and POD/DMD Analysis of Thermoacoustic Oscillation of a Hydrogen Micromix Flame Pair. In Proceedings of the Turbo Expo: Power for Land, Sea, and Air, London, UK, 24–28 June 2024; American Society of Mechanical Engineers: New York, NY, USA, 2024; Volume 87943, p. V03AT04A024 .
25. Kashir, B.; Tabejamaat, S.; Jalalatian, N. On large eddy simulation of blended CH_4–H_2 swirling inverse diffusion flames: The impact of hydrogen concentration on thermal and emission characteristics. *Int. J. Hydrog. Energy* **2015**, *40*, 15732–15748. [CrossRef]
26. Shih, H.Y.; Liu, C.R. A computational study on the combustion of hydrogen/methane blended fuels for a micro gas turbines. *Int. J. Hydrog. Energy* **2014**, *39*, 15103–15115. [CrossRef]
27. Cappelletti, A.; Martelli, F. Investigation of a pure hydrogen fueled gas turbine burner. *Int. J. Hydrog. Energy* **2017**, *42*, 10513–10523. [CrossRef]
28. Kurata, O.; Iki, N.; Inoue, T.; Matsunuma, T.; Tsujimura, T.; Furutani, H.; Kawano, M.; Arai, K.; Okafor, E.C.; Hayakawa, A.; et al. Development of a wide range-operable, rich-lean low-NO_x combustor for NH_3 fuel gas-turbine power generation. *Proc. Combust. Inst.* **2019**, *37*, 4587–4595. [CrossRef]
29. Jójka, J.; Kapela, N.; Jankowski, R.; Ślefarski, R. Analysis of the effect of swirl flame shaping on emissions from the co-firing of ammonia and methane. *Energy* **2024**, *313*, 133738. [CrossRef]
30. Ávila, C.D.; Cardona, S.; Abdullah, M.; Younes, M.; Jamal, A.; Guiberti, T.F.; Roberts, W.L. Experimental assessment of the performance of a commercial micro gas turbine fueled by ammonia-methane blends. *Appl. Energy Combust. Sci.* **2023**, *13*, 100104. [CrossRef]
31. Skabelund, B.B.; Stechel, E.B.; Milcarek, R.J. Thermodynamic analysis of a gas turbine utilizing ternary $CH_4/H_2/NH_3$ fuel blends. *Energy* **2023**, *282*, 128818. [CrossRef]
32. Bellotti, D.; Anfosso, C.; Magistri, L.; Massardo, A.F. Partially Cracked Ammonia for Micro-Gas Turbine Application. In Proceedings of the Turbo Expo: Power for Land, Sea, and Air, Boston, MA, USA, 26–30 June 2023; American Society of Mechanical Engineers: New York, NY, USA, 2023; Volume 86984, p. V005T06A032.
33. Mitsubishi Heavy Industries. 2021. Available online: https://power.mhi.com/news/20210301.html (accessed on 28 January 2025).
34. Hayakawa, A.; Goto, T.; Mimoto, R.; Arakawa, Y.; Kudo, T.; Kobayashi, H. Laminar burning velocity and Markstein length of ammonia/air premixed flames at various pressures . *Fuel* **2015**, *159*, 98–106. [CrossRef]
35. Cardoso, J.S.; Silva, V.; Rocha, R.C.; Hall, M.J.; Costa, M.; Eusébio, D. Ammonia as an energy vector: Current and future prospects for low-carbon fuel applications in internal combustion engines. *J. Clean. Prod.* **2021**, *296*, 126562. [CrossRef]
36. Yapicioglu, A.; Dincer, I. Experimental investigation and evaluation of using ammonia and gasoline fuel blends for power generators. *Appl. Therm. Eng.* **2019**, *154*, 1–8. [CrossRef]
37. Gaffin, W. NASA ECI Programs: Benefits to Pratt & Whitney Engines. In Proceedings of the Turbo Expo: Power for Land, Sea, and Air, London, UK, 18–22 March 1982; American Society of Mechanical Engineers: New York, NY, USA, 1982; Volume 79573, p. V002T02A019.
38. Evans, M.J.; Chinnici, A.; Medwell, P.R.; Dally, B.B. *Autoignition of Hydrogen/Ammonia Blends at Elevated Pressures and Temperatures*; Hydrogen Knowledge Centre: Derby/London, UK, 2019.
39. Xiao, H.; Valera-Medina, A.; Bowen, P.J. Modeling combustion of ammonia/hydrogen fuel blends under gas turbine conditions. *Energy Fuels* **2017**, *31*, 8631–8642. [CrossRef]
40. Chu, H.; Xiang, L.; Nie, X.; Ya, Y.; Gu, M.; E, J. Laminar burning velocity and pollutant emissions of the gasoline components and its surrogate fuels: A review. *Fuel* **2020**, *269*, 117451. [CrossRef]
41. Ogunfuye, S.; Perhinschi, M.; Akkerman, V. Towards a machine learning model to predict the laminar flame speed of fuel blends and vented gases in lithium-ion batteries. *Fuel* **2024**, *377*, 132712. [CrossRef]
42. Alnaeli, M.; Alnajideen, M.; Navaratne, R.; Shi, H.; Czyzewski, P.; Wang, P.; Eckart, S.; Alsaegh, A.; Alnasif, A.; Mashruk, S.; et al. High-temperature materials for complex components in ammonia/hydrogen gas turbines: A critical review. *Energies* **2023**, *16*, 6973. [CrossRef]
43. El-Adawy, M.; Nemitallah, M.A.; Abdelhafez, A. Towards sustainable hydrogen and ammonia internal combustion engines: Challenges and opportunities. *Fuel* **2024**, *364*, 131090. [CrossRef]
44. Mohammed, A.G.; Mansyur, N.; Hasini, H.; Elfeky, K.E.; Wang, Q.; Ali, M.H.; Om, N.I. Review on the ammonia-blend as an alternative fuel for micro gas turbine power generation. *Int. J. Hydrog. Energy* **2024**, *82*, 428–447. [CrossRef]
45. Horbaniuc, B.; Marin, O.; Dumitraşcu, G.; Charon, O. Oxygen-enriched combustion in supercritical steam boilers. *Energy* **2004**, *29*, 427–448. [CrossRef]

46. Nimmo, W.; Daood, S.; Gibbs, B. The effect of O_2 enrichment on NO_x formation in biomass co-fired pulverised coal combustion. *Fuel* **2010**, *89*, 2945–2952. [CrossRef]
47. Krzywański, J.; Czakiert, T.; Muskała, W.; Nowak, W. Modelling of CO_2, CO, SO_2, O_2 and NO_x emissions from the oxy-fuel combustion in a circulating fluidized bed. *Fuel Process. Technol.* **2011**, *92*, 590–596. [CrossRef]
48. Baukal, C.E., Jr. *Oxygen-Enhanced Combustion*; CRC Press: Boca Raton, FL, USA, 2010.
49. Toftegaard, M.B.; Brix, J.; Jensen, P.A.; Glarborg, P.; Jensen, A.D. Oxy-fuel combustion of solid fuels. *Prog. Energy Combust. Sci.* **2010**, *36*, 581–625. [CrossRef]
50. Ahn, S.; Choi, G.; Kim, D. The effect of wood biomass blending with pulverized coal on combustion characteristics under oxy-fuel condition. *Biomass Bioenergy* **2014**, *71*, 144–154. [CrossRef]
51. Gładysz, P.; Ziębik, A. Environmental analysis of bio-CCS in an integrated oxy-fuel combustion power plant with CO_2 transport and storage. *Biomass Bioenergy* **2016**, *85*, 109–118. [CrossRef]
52. Riaza, J.; Khatami, R.; Levendis, Y.A.; Álvarez, L.; Gil, M.V.; Pevida, C.; Rubiera, F.; Pis, J.J. Combustion of single biomass particles in air and in oxy-fuel conditions. *Biomass Bioenergy* **2014**, *64*, 162–174. [CrossRef]
53. Smart, J.P.; Patel, R.; Riley, G.S. Oxy-fuel combustion of coal and biomass, the effect on radiative and convective heat transfer and burnout. *Combust. Flame* **2010**, *157*, 2230–2240. [CrossRef]
54. Gil, M.V.; Riaza, J.; Álvarez, L.; Pevida, C.; Pis, J.; Rubiera, F. Kinetic models for the oxy-fuel combustion of coal and coal/biomass blend chars obtained in N_2 and CO_2 atmospheres. *Energy* **2012**, *48*, 510–518. [CrossRef]
55. Zhu, C.; Liu, S.; Liu, H.; Yang, J.; Liu, X.; Xu, G. NOx emission characteristics of fluidized bed combustion in atmospheres rich in oxygen and water vapor for high-nitrogen fuel. *Fuel* **2015**, *139*, 346–355. [CrossRef]
56. General Electric, USA . GE LM6000 Gas Turbine Overview. 2025. Available online: https://www.gevernova.com/gas-power/products/gas-turbines/lm6000 (accessed on 27 January 2025).
57. Roy, P.S.; Amin, M.R. Aspen-HYSYS simulation of natural gas processing plant. *J. Chem. Eng.* **2011**, *26*, 62–65. [CrossRef]
58. Aydin, H. Exergetic sustainability analysis of LM6000 gas turbine power plant with steam cycle. *Energy* **2013**, *57*, 766–774. [CrossRef]
59. Shrestha, K.P.; Eckart, S.; Elbaz, A.M.; Giri, B.R.; Fritsche, C.; Seidel, L.; Roberts, W.L.; Krause, H.; Mauss, F. A comprehensive kinetic model for dimethyl ether and dimethoxymethane oxidation and NOx interaction utilizing experimental laminar flame speed measurements at elevated pressure and temperature. *Combust. Flame* **2020**, *218*, 57–74. [CrossRef]
60. Shrestha, K.P.; Eckart, S.; Drost, S.; Fritsche, C.; Schießl, R.; Seidel, L.; Maas, U.; Krause, H.; Mauss, F. A comprehensive kinetic modeling of oxymethylene ethers (OMEn, n = 1–3) oxidation-laminar flame speed and ignition delay time measurements. *Combust. Flame* **2022**, *246*, 112426. [CrossRef]
61. Kee, R.J.; Miller, J.A.; Evans, G.H.; Dixon-Lewis, G. A computational model of the structure and extinction of strained, opposed flow, premixed methane-air flames. In Proceedings of the Symposium (International) on Combustion, Hollywood, FL, USA, 11–14 April 1989; Elsevier: Amsterdam, The Netherlands, 1989; Volume 22, pp. 1479–1494.
62. Kee, R.J.; Rupley, F.M.; Meeks, E.; Miller, J.A. *CHEMKIN-III: A FORTRAN Chemical Kinetics Package for the Analysis of Gas-Phase Chemical and Plasma Kinetics*; Technical Report; Sandia National Lab. (SNL-CA): Livermore, CA, USA, 1996.
63. Božo, M.G.; Mashruk, S.; Zitouni, S.; Valera-Medina, A. Humidified ammonia/hydrogen RQL combustion in a trigeneration gas turbine cycle. *Energy Convers. Manag.* **2021**, *227*, 113625. [CrossRef]
64. Vigueras-Zuniga, M.O.; Tejeda-del Cueto, M.E.; Vasquez-Santacruz, J.A.; Herrera-May, A.L.; Valera-Medina, A. Numerical predictions of a swirl combustor using complex chemistry fueled with ammonia/hydrogen blends. *Energies* **2020**, *13*, 288. [CrossRef]
65. Valera-Medina, A.; Syred, N.; Bowen, P. Central recirculation zone visualization in confined swirl combustors for terrestrial energy. *J. Propuls. Power* **2013**, *29*, 195–204. [CrossRef]
66. Mével, R.; Javoy, S.; Coudoro, K.; Dupré, G.; Paillard, C.E. Assessment of H_2-CH_4-air mixtures oxidation kinetic models used in combustion. *Int. J. Hydrog. Energy* **2012**, *37*, 698–714. [CrossRef]
67. Alnasif, A.; Mashruk, S.; Shi, H.; Alnajideen, M.; Wang, P.; Pugh, D.; Valera-Medina, A. Evolution of ammonia reaction mechanisms and modeling parameters: A review. *Appl. Energy Combust. Sci.* **2023**, *15*, 100175.
68. Samuelsen, G.; Brouwer, J.; Vardakas, M.; Holdeman, J. Experimental and modeling investigation of the effect of air preheat on the formation of NO_x in an RQL combustor. *Heat Mass Transf.* **2013**, *49*, 219–231. [CrossRef]
69. Feitelberg, A.; Lacey, M. The GE rich-quench-lean gas turbine combustor. *J. Eng. Gas Turbines Power* **1998**, *120*, 502–508. [CrossRef]
70. Lee, J.E.; Shafiq, I.; Hussain, M.; Lam, S.S.; Rhee, G.H.; Park, Y.K. A review on integrated thermochemical hydrogen production from water. *Int. J. Hydrog. Energy* **2022**, *47*, 4346–4356. [CrossRef]
71. Arsalis, A. Thermodynamic modeling and parametric study of a small-scale natural gas/hydrogen-fueled gas turbine system for decentralized applications. *Sustain. Energy Technol. Assess.* **2019**, *36*, 100560. [CrossRef]
72. Lopez-Ruiz, G.; Castresana-Larrauri, J.; Blanco-Ilzarbe, J.M. Thermodynamic analysis of a regenerative brayton cycle using H_2, CH_4 and H_2/CH_4 blends as fuel. *Energies* **2022**, *15*, 1508. [CrossRef]

73. Shi, X.; Lian, T.; Zhang, Y.; Liu, Z.; Li, W.; Xi, Z.; Li, Y. Enhanced ammonia combustion by partial pre-cracking strategy in a gas turbine model combustor: Flame macrostructures, lean blowout characteristics and exhaust emissions. *Appl. Energy Combust. Sci.* **2024**, *17*, 100247. [CrossRef]
74. González, M.S.; Rojas-Hernández, I. Hydrogen embrittlement of metals and alloys in combustion engines. *Tecnol. Marcha* **2018**, *31*, 3–13.
75. Ghara, T.; Kuroda, S.; Yanagisawa, T.; Shahien, M.; Suzuki, M.; Inoue, T.; Shinoda, K. Degradation behaviour of HVOF sprayed CoNiCrAlY coating in high-temperature ammonia environment towards its applicability in ammonia fueled gas turbines. *Int. J. Hydrog. Energy* **2025**, *130*, 345–359. [CrossRef]
76. Davalos-Monteiro, R. Observations of corrosion product formation and stress corrosion cracking on brass samples exposed to ammonia environments. *Mater. Res.* **2018**, *22*, e20180077. [CrossRef]
77. Smialek, J.L.; Miller, R.A. Revisiting the birth of 7YSZ thermal barrier coatings: Stephan Stecura. *Coatings* **2018**, *8*, 255. [CrossRef]